THE JOURNAL OF BIOLOGICAL CHEMISTRY VOL. 291, NO. 53, pp. 27371–27386, December 30, 2016

Dissociation of Golgi-associated DHHC-type Zinc Finger Protein (GODZ)- and Sertoli Cell Gene with a Zinc Finger Domain-β (SERZ-β)-mediated Palmitoylation by Loss of Function Analyses in Knock-out Mice*

Received for publication, April 15, 2016, and in revised form, September 28, 2016 Published, JBC Papers in Press, November 14, 2016, DOI 10.1074/jbc.M116.732768

Casey L. Kilpatrick[‡1], **Shoko Murakami**[§1], **Mengyang Feng**[§], **Xia Wu**[§], **Rachnanjali Lal**[§], **Gong Chen**[§¶], **Keyong Du**[‖], **and Bernhard Luscher**[‡§¶2]

From the Departments of [‡]*Biochemistry and Molecular Biology and* [§]*Biology and the* [¶]*Center for Molecular Investigation of Neurological Disorders (CMIND), Pennsylvania State University, University Park, Pennsylvania 16802 and* [‖]*Molecular Oncology Research Institute, Tufts Medical Center, Boston, Massachusetts 02111*

Edited by F. Anne Stephenson

The γ2 subunit of GABA type A receptors ($GABA_A$Rs) is thought to be subject to palmitoylation by both Golgi-associated DHHC-type zinc finger protein (GODZ; also known as DHHC3) and its paralog Sertoli cell gene with a zinc finger domain-β (SERZ-β; DHHC7) based on overexpression of enzymes and substrates in heterologous cells. Here we have further investigated the substrate specificity of these enzymes by characterization of GODZ and SERZ-β knock-out (KO) mice as well as double KO (DKO) neurons. Palmitoylation of γ2 and a second substrate, growth-associated protein of 43 kDa, that is independently implicated in trafficking of $GABA_A$Rs was significantly reduced in brain of GODZ KO *versus* wild-type (WT) mice but unaltered in SERZ-β KO mice. Accumulation of $GABA_A$Rs at synapses, GABAergic innervation, and synaptic function were reduced in GODZ KO and DKO neurons to a similar extent, indicating that SERZ-β does not contribute to palmitoylation or trafficking of $GABA_A$Rs even in the absence of GODZ. Notably, these effects were seen only when mutant neurons were grown in competition with WT neurons, thereby mimicking conditions of shRNA-transfected neurons previously used to characterize GODZ. However, GABA-evoked whole-cell currents of DKO neurons and the $GABA_A$R cell surface expression in DKO neurons and GODZ or SERZ-β KO brain slices were unaltered, indicating that GODZ-mediated palmitoylation selectively controls the pool of receptors at synapses. The different substrate specificities of GODZ and SERZ-β *in vivo* were correlated with their differential localization to cis- *versus* trans-Golgi compartment, a mechanism that was compromised by overexpression of GODZ.

S-Palmitoylation is an important posttranslational modification that involves the addition of the 16-carbon fatty acid chain palmitate via a thioester bond to Cys residues (1). This modification in turn can alter a protein's conformational state, membrane association, and complex formation as well as its susceptibility to other posttranslational modifications (2–4). Global analyses of rat synaptosomal fractions led to the discovery of nearly 300 palmitoylated synaptosomal protein candidates that illustrate the particular importance of palmitoylation in regulating the function of neuronal synapses (5).

In mammalian cells, the palmitoylation reaction is catalyzed principally by a super gene family of 23 palmitoyl acyltransferases containing a DHHC motif in a cysteine-rich domain (DHHC-CRD)[3] that are both essential for enzyme function (6–10). The mechanisms that determine substrate specificity of PATs remain poorly understood, although some specificity is observed upon overexpression of substrates and PATs in heterologous cells. However, increasing evidence suggests that the substrate specificity of DHHC-type PATs *in vivo* is much more stringent than *in vitro*. For example, the postsynaptic density (PSD) protein of 95-kDa (PSD-95) can be palmitoylated in heterologous cells by at least five members of the DHHC family of PATs (11), whereas *in vivo* only DHHC8 and DHHC2 have so far been shown to be required for normal palmitoylation of PSD-95 (12, 13). In part, the substrate specificity of DHHC enzymes may be determined by their segregation to different subcellular compartments, which has also implications as to how palmitoylation affects the trafficking or function of substrate proteins (14).

* This work was supported by National Institutes of Health Grants MH62391 and MH062391 (to B. L.), MH083911 (to G. C.), DK084319 (to K. D.), and OD010625 (to Simon Watkins, Center for Biologic Imagining at the University of Pittsburgh, PA) and by a grant from the Pennsylvania Department of Health using Tobacco Settlement Funds. The authors declare that they have no conflicts of interest with the contents of this article. The content is solely the responsibility of the authors and does not necessarily represent the official views of the National Institutes of Health.

[1] Both authors contributed equally to this work.

[2] To whom correspondence should be addressed: Dept. of Biology, Pennsylvania State University, 209 Life Sciences Bldg., University Park, PA 16802. Tel.: 814-865-5549; E-mail: BXL25@psu.edu.

[3] The abbreviations used are: DHHC-CRD, DHHC motif in a cysteine-rich domain; $GABA_A$R, GABA type A receptor; GODZ, Golgi-associated DHHC-type zinc finger protein; SERZ-β, Sertoli cell gene with a zinc finger domain-β; DKO, double KO; GAP-43, growth-associated protein of 43 kDa; PAT, palmitoyl acyltransferase; PSD, postsynaptic density; AMPAR, AMPA receptor; DIV, days *in vitro*; GAD, glutamic acid decarboxylase; n.s., nonsignificant; ANOVA, analysis of variance; mEPSC, miniature excitatory postsynaptic current; mIPSC, miniature inhibitory postsynaptic current; ABE, acyl-biotin exchange; GalT, galactosyltransferase; SIM, structured illumination microscopy; ICQ, intensity correlation quotient; PGK-neo, phosphoglycerate kinase-neomycin resistance gene cassette; BAC, bacterial artificial chromosome; NHS, *N*-hydroxysuccinimide; ACSF, artificial cerebrospinal fluid; NA, numerical aperture.

Here we have extended our characterization of GODZ (also known as DHHC3) and its most closely related paralog, Sertoli cell gene with a zinc finger domain-β (SERZ-β; DHHC7), which are known as founding members of the mammalian DHHC family of proteins (15, 16). We have previously provided evidence that in cultured neurons GODZ is important as a PAT of γ2 subunit-containing γ-aminobutyric acid (GABA) type A receptors ($GABA_A$Rs), the principal receptors that mediate GABAergic synaptic inhibition (17). Moreover, GODZ shRNA- or dominant negative GODZ-mediated knockdown of GODZ suggested that GODZ functions selectively at inhibitory but not excitatory synapses (18). Nevertheless, GODZ has independently been proposed to also regulate the trafficking of ionotropic glutamate receptors as both AMPA and NMDA receptors can be palmitoylated upon overexpression of GODZ in heterologous cells and neurons (19, 20).

Based on mRNA expression analyses, GODZ and SERZ-β show similar tissue-specific expression *in vivo* and in brain are selectively expressed in neurons (18). When examined by overexpression in heterologous cells, both enzymes exhibit broad substrate specificity, and indeed virtually any palmitoylated protein can be palmitoylated by both GODZ and SERZ-β under these conditions (11, 18, 21). However, the extent by which any of these putative substrate proteins are palmitoylated by GODZ or SERZ-β *in vivo* has not been addressed.

To begin to address the role GODZ-mediated palmitoylation plays by loss of function analyses *in vivo*, here we have generated GODZ and SERZ-β knock-out (KO) mice. Analyses of GODZ KO and GODZ/SERZ-β double KO (DKO) primary cultured neurons confirmed that GODZ is important for normal accumulation of $GABA_A$Rs at synapses and receptor-dependent presynaptic innervation. However, this phenotype was only observed when mutant neurons were grown and analyzed under conditions where they were forced to compete with wild-type (WT) neurons for GABAergic innervation, *i.e.* conditions we previously showed to be highly sensitive to reduced expression of the γ2 subunit of $GABA_A$Rs (22). By contrast, the cell surface expression and synaptic localization of $GABA_A$Rs and the density of GABAergic synapses were unaffected in pure DKO cultures. Nevertheless, palmitoylation of γ2 was markedly reduced in brain of GODZ KO compared with WT mice along with reduced palmitoylation of growth-associated protein of 43 kDa (GAP-43) (also known as neuromodulin) as a second substrate that was recently implicated in the formation of GABAergic synapses (23). Consistent with all these findings, electrophysiological analyses of DKO neurons revealed functional defects that were principally limited to inhibitory synapses. Notably, palmitoylation of PSD-95 and AMPARs was unaltered in brain of GODZ and SERZ-β KO mice. Moreover, palmitoylation of γ2 and GAP-43 was unaltered in SERZ-β KO mice. The data indicate substantially greater substrate specificity of both PATs *in vivo versus in vitro*. Super-resolution microscopy showed that GODZ is highly restricted to the cis-Golgi, whereas SERZ-β was enriched in the trans-Golgi. Such differences in the subcellular localization of PATs might contribute to the increased substrate specificity of these enzymes *in vivo versus* after overexpression of substrate and enzyme in heterologous cells.

Results

Generation and Verification of GODZ and SERZ-β Knock-out Mice—To enable investigation of the role of GODZ- and SERZ-β-mediated palmitoylation by loss of function analyses *in vivo*, we generated KO mice in which the third and fourth protein-encoding exons of each of these two genes were deleted by homologous recombination in embryonic stem cells (Fig. 1, *a* and *b*, and "Experimental Procedures"). These two exons together encode the DHHC-CRD that is essential for enzyme function of GODZ and other DHHC family PATs (9, 10). For both GODZ and SERZ-β, deletion of exons 3 and 4 is predicted to cause a shift in the translational reading frame of the downstream exons with artificial stop sites and hence to result in enzymatically inactive, truncated, and likely unstable proteins that contain the protein sequence of only the first two of a total of six protein-coding exons. Successful deletion of exons 3 and 4 was verified by Southern blotting of genomic DNA using DNA probes that flanked the targeting vector (not shown) and by reverse transcription (RT)-PCR analyses of total brain RNA (Fig. 1*c*). For each gene, RT-PCR of RNA isolated from WT and heterozygous mice using primer pairs that annealed to exons 1 and 4 (GP1/2 and SP1/2, respectively; Fig. 1, *a* and *b*) revealed the expected RT-PCR amplification products in WT mice that were absent from corresponding KO mice as expected (Fig. 1*c*, *upper micrographs*, primer pairs GP1/2 and SP1/2). Moreover, PCR analyses of reverse transcribed RNA using primers that annealed to exons 1 and 6 of each gene (GP1/3 and SP1/3, respectively; Fig. 1, *a* and *b*) revealed the presence of the predicted cDNAs of WT mice and the predicted truncated products corresponding to cDNAs that had exons 3 and 4 deleted (Fig. 1*c*, *lower micrographs*, primer pairs GP1/3 and SP1/3). RNA isolated from heterozygous GODZ and SERZ-β mice gave rise to both the WT and truncated RT-PCR products as expected (Fig. 1*c*).

Next we confirmed the absence of GODZ in KO mice by Western blotting (Fig. 1*d*, *left panels*). Immunoblotting of whole brain lysates of WT and SERZ-β KO mice probed for GODZ detected a ~31-kDa protein corresponding in size to previously described epitope-tagged recombinant GODZ, which is slightly smaller than predicted based on its 299-amino acid sequence (17). Importantly, this protein was absent in brain lysates of GODZ KO mice as expected (Fig. 1*d*, *left panels*). Immunoblots for heat shock protein of 90 kDa (HSP90) analyzed in parallel were used as loading controls (Fig. 1*d*, *lower panels*). Notably, the GODZ antiserum used for Western blotting was directed against a C-terminal 31-amino acid peptide of GODZ that is absent in the putative truncated protein of GODZ KO mice because of the deletion-induced, altered translational reading frame.

Parallel analyses of the same brain lysates with a SERZ-β antiserum detected a protein with an M_r of ~30,000, which again is slightly less than the predicted molecular weight for this 308-amino acid protein. As predicted, this protein was present in extracts of WT and GODZ KO mice and absent in SERZ-β KO mice (Fig. 1*d*, *right panels*). The SERZ-β antiserum used for these experiments is directed against a peptide containing amino acids 40–193 of human SERZ-β that includes a 37-

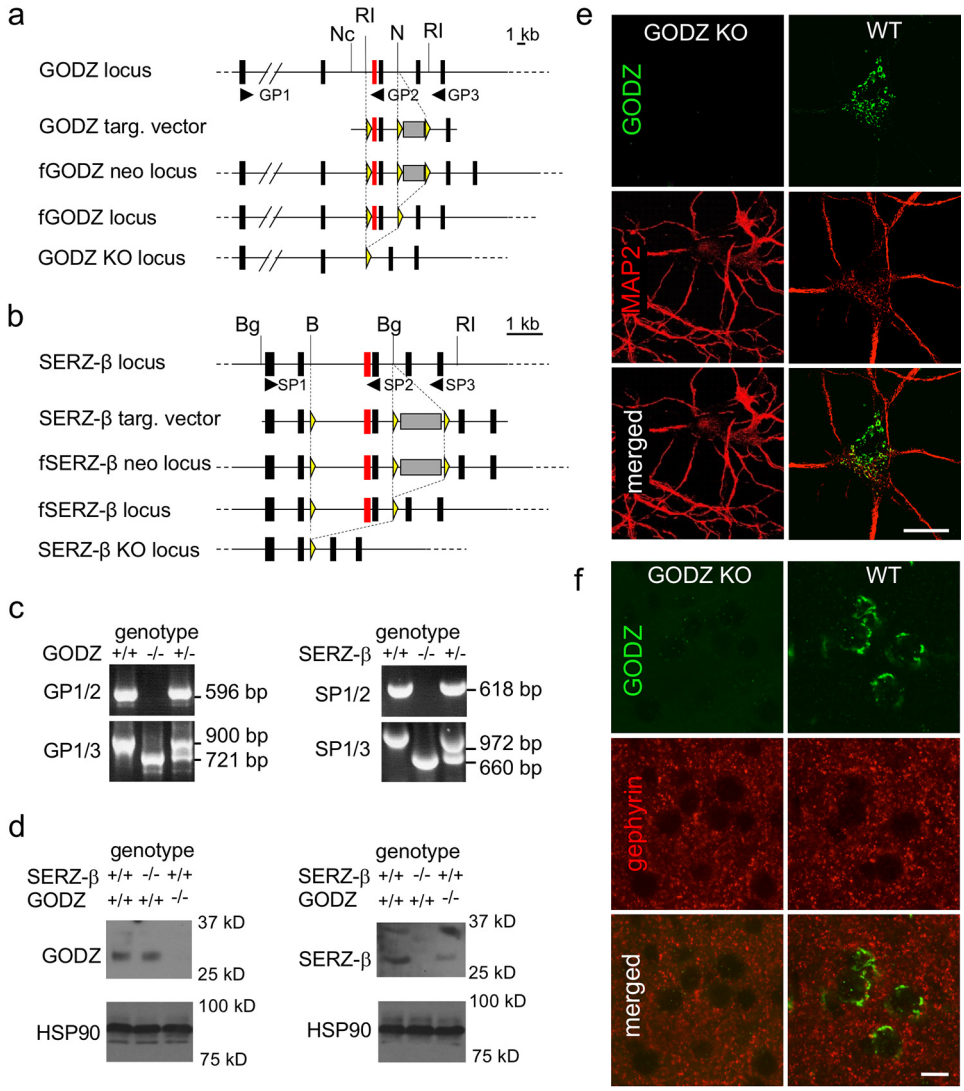

FIGURE 1. **Strategy and verification of targeted inactivation of the GODZ and SERZ-β loci.** *a* and *b*, schematic representations of the targeted (*targ.*) genomic regions of GODZ (*a*) and SERZ-β (*b*) showing from *top* to *bottom* (i) the genomic loci including the protein-coding exons of GODZ and SERZ-β, respectively (exons are shown as *black boxes* except for the DHHC domain-containing exons that are essential for enzymatic activity and shown in *red*), (ii) targeting vectors, (iii) mutated alleles resulting from homologous recombination, (v) the floxed alleles after Cre-mediated deletion of the PGK-neo cassette (*gray shaded box*), and the mutated alleles lacking the fourth and fifth protein-coding exons. The *yellow triangles* indicate the positions of the loxP sites. The locations of the primers used for RT-PCR analyses (GP1–3 for GODZ and SP1–3 for SERZ-β; shown in 5′–3′ direction) are indicated as *black arrowheads*. Exons are shown larger than to scale. For simplicity, the exons coding for non-translated region of the mRNAs are not shown. Restriction sites are indicated as follows: *B*, BamHI; *Bg*, BglII; *RI*, EcoRI; *N*, NcoI. *c*, RT-PCR analyses of brain RNA from GODZ (*left*) and SERZ-β (*right*) KO mice with the genotypes analyzed indicated at the *top* of panels, the primer pairs (GP1–3 and SP1–3) used indicated on the *left*, and the size of amplified cDNA fragments representing WT and KO alleles for each primer pair indicated on the *right*. *d*, immunoblots of brain lysates of GODZ and SERZ-β KO mice probed with antibodies raised against GODZ and SERZ-β and genotypes as indicated. Note the absence of GODZ- and SERZ-β-specific bands of ~31 and ~30 kDa in lysates of GODZ KO and SERZ-β KO mice, respectively. The SERZ-β antiserum in addition to the ~30-kDa bands recognizes a ~36-kDa SERZ-β-related protein species, both absent in SERZ-β KO mice. *e*, representative images of cultured cortical neurons derived from WT and homozygous GODZ KO mice immunostained for GODZ (*green*; *top*) and MAP2 (*red*; *middle*) with merged images shown at the *bottom*. *f*, immunostaining of cortical brain sections of a WT (*left column*) and GODZ KO mouse (*right column*) for GODZ (*green*; *top*) and gephyrin (*red*; *middle*) with merged images shown in the *bottom row*. Note the absence of the GODZ immunoreactivity in cultured neurons and brain sections of GODZ KO mice. *Scale bars*, 10 μm.

amino acid exon that is absent in mouse SERZ-β, whereas the rest of the immunogen is 98% conserved between human and mouse. In addition to the expected ~30-kDa SERZ-β protein species, this antiserum detected an additional, more slowly migrating SERZ-β-immunoreactive band (~35 kDa) that was also absent in SERZ-β KO mice and therefore may be SERZ-β-related (Fig. 1*d*, *right panels*). It could represent a detergent-resistant complex of SERZ-β with another, as of yet unknown protein.

Next we verified the absence of GODZ immunoreactivity from cultured GODZ KO neurons and brain sections using a GODZ antibody directed against the C-terminal 50-amino acid peptide of mouse GODZ. Immunostaining for the microtubule-associated protein MAP2 was used to illustrate the outlines of neurons and dendrites. Immunofluorescent staining of primary cultured cortical neurons at 18 days *in vitro* (DIV 18) confirmed the Golgi-specific staining of GODZ described previously (17). Moreover, this staining was entirely absent in cultures prepared from GODZ KO embryos (Fig. 1*e*). In brain sections of WT mice, GODZ immunoreactivity was similarly delimited to Golgi-like structures of neurons as expected, and

this staining was absent in sections of GODZ KO mice (Fig. 1*f*). Immunostaining for the inhibitory synapse marker gephyrin was used to visually delineate the neuropil from neuronal somata of brain sections. Notably, analogous immunostainings for SERZ-β were not feasible as the SERZ-β antiserum used for Western blotting revealed only unspecific staining under these (non-denaturing) conditions (not shown). Nevertheless, all our analyses were consistent with faithful and specific inactivation of the GODZ and SERZ-β genomic loci in the respective KO mice.

The Phenotype of Double KO Mice Suggests Functional Redundancy of GODZ and SERZ-β in Vivo—Both GODZ KO and SERZ-β KO mice were found to be viable and fertile without overt behavioral or physical phenotypes. Nevertheless, male GODZ KO mice showed a modest reduction in body weight (89.2 ± 2.5% of WT at 1 month of age, $p < 0.001$; 90.4 ± 1.7% of WT at 2 months of age, $p < 0.01$; $n = 14–18$ for all groups, *t* tests). By contrast, the body weights of female GODZ KO mice and male and female SERZ-β KO mice were not measurably affected (not shown). Previous *in vitro* experiments using overexpression of recombinant proteins had indicated largely overlapping substrate specificity of GODZ and SERZ-β (Ref. 18; and for review, see Ref. 6). Therefore, to test for possible functional redundancy of GODZ and SERZ-β, we interbred GODZ and SERZ-β KO mice to generate GODZ/SERZ-β DKO mice. Unexpectedly, most DKO mice showed a perinatally lethal phenotype, although early on during the course of these studies a few DKO mice survived to adulthood. By 1 year of age these surviving DKO mice showed drastically reduced body and brain weights when compared with littermate controls (total body weight of DKO mice, 53.6 ± 1.7% of GODZ$^{+/-}$ SERZ-$\beta^{+/-}$ and GODZ$^{+/+}$ SERZ-$\beta^{-/-}$ controls; DKO brain weight, 74.7 ± 6.3% of controls; $n = 3$ mice/group). No viable postnatal DKO mice were recovered beyond three generations of brother-sister matings of GODZ$^{+/-}$ SERZ-$\beta^{+/-}$ mice. As predicted, these findings suggested at least partial functional redundancy of GODZ and SERZ-β and, by extension, significant overlap in substrate specificity of these two enzymes. In addition, they dictated that further analyses of the neuronal mutant phenotypes were limited to single KO mice or to cultured neurons derived from KO or DKO embryos.

GODZ Is Required for Normal Trafficking of $GABA_A$Rs and for GABAergic Innervation—Given the defects in $GABA_A$R clustering and synapse formation seen previously in shRNA- and dominant negative GODZ-transfected neurons (18), we predicted that such deficits should be replicated in neuron cultures prepared from GODZ KO neurons. Surprisingly, cortical neurons prepared from GODZ KO embryos (18 DIV) showed normal $GABA_A$R clustering as evidenced by unaltered density of punctate immunostaining for the γ2 subunit and the presynaptic marker glutamic acid decarboxylase (GAD) in GODZ KO compared with WT cortical cultures (Fig. 2, *a–d versus e–h*, *m*, and *n*) (mean number of γ2 puncta/40 μm dendrite: WT, 17.5 ± 1.1, GODZ KO, 16.8 ± 0.9; *p*, n.s.; $n = 12–17$ cells, analyses of variance (ANOVA); mean number of GAD puncta/40 μm dendrite: WT, 14.8 ± 1.3, GODZ KO, 14.8 ± 1.1; *p*, n.s.; $n = 12–17$, ANOVA). Similarly, inhibitory synapse formation was unaffected as indicated by normal colocalization of punctate postsynaptic γ2 staining and presynaptic GAD immunoreactivity (colocalization of γ2 with GAD in WT 92.0 ± 3.1% *versus* GODZ KO 90.0 ± 4.2%; *p*, n.s.; $n = 12–18$, ANOVA) (Fig. 2, *a–d versus* e–*h* and *o*).

The normal density of $GABA_A$Rs clusters and inhibitory synapses in KO cultures at first appeared to conflict with our previous results obtained by shRNA- or dominant negative GODZ-mediated knockdown of GODZ that suggested a role for GODZ in clustering of $GABA_A$Rs and inhibitory synapse formation (18). However, we recently showed that γ2-$GABA_A$Rs are critically important for GABAergic synapse formation selectively under conditions where $GABA_A$R-deficient neurons are forced to compete with WT neurons for presynaptic innervation by WT neurons (22), *i.e.* conditions that mimic cultures that were sparsely transfected with shRNA constructs. Thus, to assess whether GODZ was required for inhibitory synapse formation under competitive conditions, we co-cultured GODZ KO neurons with WT neurons (1:9 ratio). WT neurons were prepared from a GFP transgenic embryo to facilitate distinction of mutant and WT neurons. Interestingly, under these conditions, GODZ KO neurons showed drastically reduced density of puncta for the γ2 subunit and GAD compared with WT cultures (density of puncta in KO neurons mixed with WT neurons as a percentage of pure WT cultures: γ2, 57.5 ± 4.9%; GAD, 57.9 ± 4.0%; $p < 0.001$, $n = 10–12$ cells for both comparisons, ANOVA, Tukey tests) (for absolute values, see Fig. 3, *m* and *n*) (Fig. 3, *a–d versus i–l*, *m*, and *n*). Residual $GABA_A$R clusters in mutant neurons of mixed cultures remained invariably colocalized with presynaptic GAD (percent colocalization: GODZ KO/WT co-cultures, 89.2 ± 4.3%; WT pure cultures, 91.9 ± 3.0%; *p*, n.s.; $n = 12–18$, ANOVA) (Fig. 3*o*). Notably, our analyses of mutant neurons focused on pyramidal shaped neurons that lacked somatic GAD immunoreactivity and GFP fluorescence. Therefore, the GABAergic terminals contacting mutant neurons in these mixed genotype cultures originated almost exclusively from WT neurons, and the synaptic phenotypes of mutant pyramidal cells can be attributed specifically to postsynaptic defects in palmitoylation. The data indicate that GODZ KO neurons replicate the phenotype previously described for GODZ shRNA- and GODZ dominant negative construct-transfected cultures.

Unaltered clustering of the γ2 subunit in (pure) GODZ KO cultures was unexpected and appeared inconsistent with a simple role of palmitoylation in forward trafficking of $GABA_A$Rs to the plasma membrane, raising the possibility of functional redundancy of GODZ with SERZ-β. To further assess whether the phenotype of GODZ KO neurons was compromised by functional redundancy between GODZ and SERZ-β, we repeated the above experiments with neuron cultures prepared from DKO (GODZ$^{-/-}$ SERZ-$\beta^{-/-}$) embryos. Similar to results obtained with GODZ KO cultures, cortical cultures (18 DIV) prepared from pure DKO embryos showed normal density and colocalization of punctate immunoreactivity for the γ2 subunit and GAD (density as percentage of WT: γ2, 97.4 ± 3.1%; GAD, 96.2 ± 3.6%; *p*, n.s.; $n = 29–46$ cells; colocalization of γ2 and GAD: DKO, 87.2 ± 1.5%; WT, 87.3 ± 1.9%; $n = 30–46$; *p*, n.s.; ANOVA) (Fig. 3, *a–e versus e–h* and *m–o*). Moreover, DKO neurons co-cultured with GFP-tagged WT neurons showed

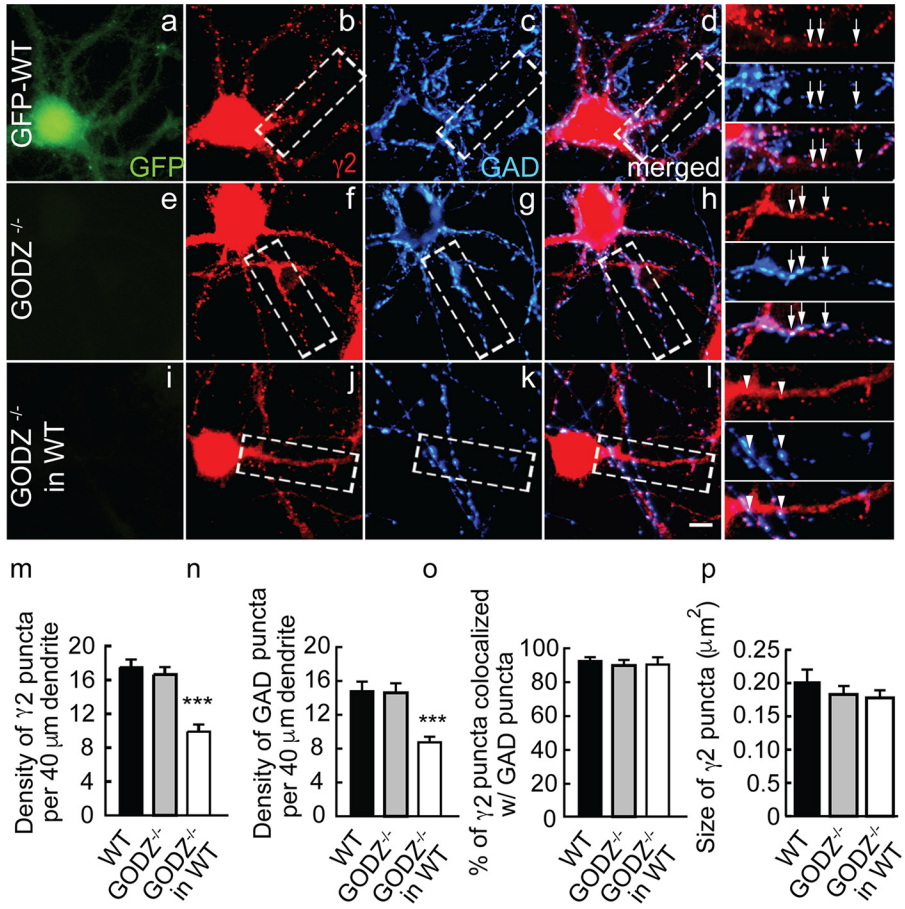

FIGURE 2. **Deficits in $GABA_AR$ postsynaptic clustering and inhibitory synapse density in GODZ KO cortical neurons co-cultured with WT neurons.** GFP-transgenic WT cultures and GODZ KO cortical neurons were cultured as pure cultures, or the mutant neurons were co-cultured 1:9 with an excess of GFP-expressing WT neurons. GFP autofluorescence was used to distinguish WT from mutant neurons. *a–l*, representative micrographs of a GFP-WT neuron (*a–d*; note the GFP autofluorescence in *a* (*green*)), a GODZ KO neuron (*e–h*), and a GODZ KO neuron co-cultured with WT neurons (*i–l*) immunostained for the γ2 subunit (*b*, *f*, and *j*; *red*) and GAD (*c*, *g*, and *k*; *blue*) with corresponding merged images shown in *d*, *h*, and *l*. *Boxed* dendritic segments are shown enlarged in the *right-most column* of micrographs with *arrows* pointing to colocalized pre- and postsynaptic structures of axons that have grown along and seem to adhere to dendrites and *arrowheads* pointing to axons (*blue*) that have grown across dendrites with minimal contact. *m–p*, summary quantifications of the density of γ2 (*m*) and GAD (*n*) immunoreactive puncta, their colocalization (*o*), and the size of γ2 puncta (*p*). Note the drastic reduction in the density of both pre- and postsynaptic structures selectively in GODZ KO neurons that were grown in the presence of an excess of WT neurons, whereas the density of puncta in pure KO cultures remained unaffected. In mutant neurons grown in competition with WT neurons, the defect in synaptic localization of $GABA_ARs$ resulted in loss of innervation by WT neurons. Bar graphs with *error bars* indicate means ± S.E. ***, $p < 0.001$, ANOVA, Tukey tests. *Scale bar*, 5 μm.

defects in pre- and postsynaptic clustering comparable with GODZ KO/WT co-cultures described above (density of puncta in DKO/WT co-cultures as a percentage of pure WT cultures: γ2, 49.7 ± 1.9%, $n = 30–59$; GAD, 55.3 ± 2.2%, $n = 29–59$; $p < 0.001$, ANOVA, Tukey tests) (Fig. 3, *e–h versus i–l*, *m*, and *n*). However, unlike in the case of GODZ KO/WT co-cultures, neurons of DKO/WT co-cultures showed significantly reduced colocalization of punctate γ2 and GAD immunoreactivities (colocalization in DKO/WT co-cultures as a percentage of pure WT neurons, 82.6 ± 2.9; $p < 0.001$, $n = 30–59$) (Fig. 3*o*). The size of γ2 puncta in DKO neurons of DKO/WT co-cultures remained unaltered (DKO neurons co-cultured, 96.8 ± 5.6% of WT; *p*, n.s.; $n = 30–59$, ANOVA). The data suggest that the reduced density of puncta observed in GODZ KO and GODZ/SERZ-β DKO neurons that was observed selectively in co-cultures was not simply a consequence of reduced forward trafficking of $GABA_ARs$ to the cell surface. Curiously, quantitative comparison of the γ2 clustering defect observed in co-cultured GODZ KO neurons (density of γ2 puncta in GODZ KO, 57.5% of WT) with the defect observed in co-cultured DKO neurons (density of γ2 puncta in DKO, 49.7% of WT) revealed no significant difference (*p*, n.s; $n = 30–59$ (DKO) and $n = 12–18$ (GODZ KO), two-way ANOVA) and indicated that SERZ-β did not contribute to palmitoylation and trafficking of γ2-$GABA_ARs$ even in the absence of GODZ (*i.e.* in GODZ KO neurons). Hence, although the lethal phenotype of DKO mice suggests functional redundancy of GODZ and SERZ-β with respect to at least some of their substrates, no such overlap in function is apparent with respect to $GABA_AR$ clustering.

GODZ Is Required for Normal Function of Inhibitory Synapses—To corroborate the above findings of altered inhibitory synapses with functional assays, we performed patch clamp recordings of DKO neurons grown in competition with GFP-transgenic WT neurons, analogous to conditions used for immunostaining above. Whole-cell currents evoked by 20-s 100 μM GABA pulses recorded from DKO neurons (3741 ± 651 pA) were indistinguishable from whole-cell currents recorded from WT neurons in the same culture (4418 ± 770 pA; $n = 12$, $p > 0.05$) (Fig. 4*a*), suggesting normal cell surface expression of $GABA_ARs$. Similarly, whole-cell glutamate-evoked currents

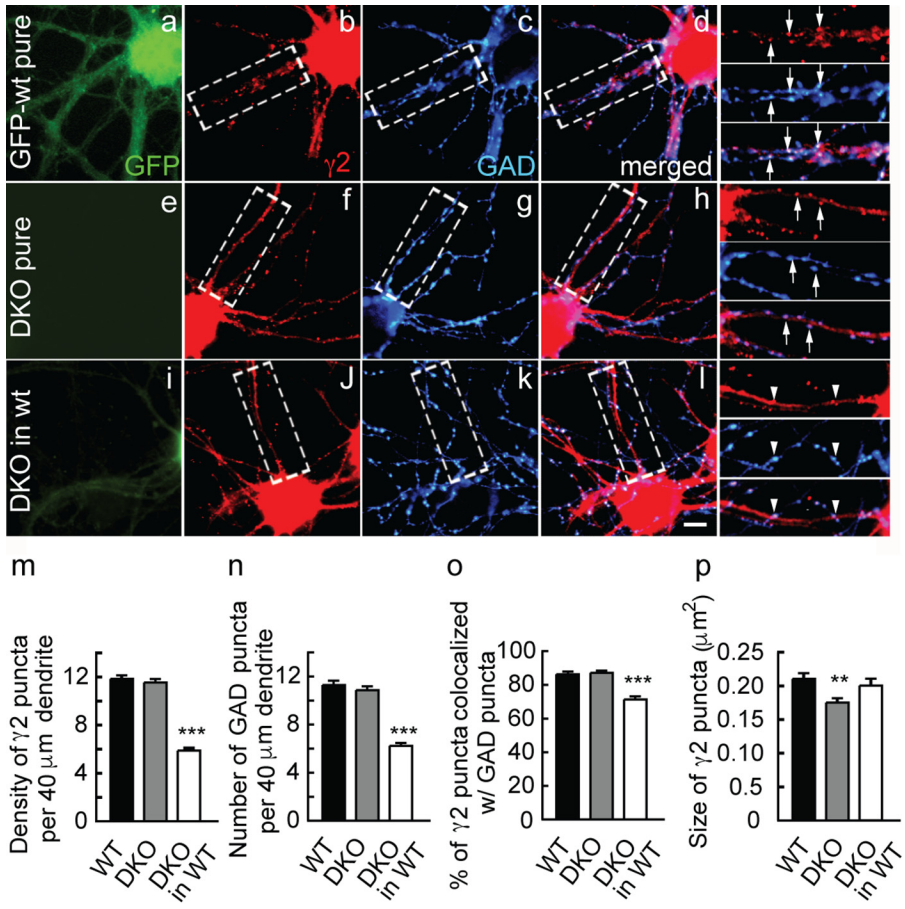

FIGURE 3. **Deficits in $GABA_AR$ postsynaptic clustering and inhibitory synapse density in DKO cortical neurons co-cultured with WT neurons.** DKO cortical neurons were cultured on their own or co-cultured 1:9 with an excess of GFP-expressing WT neurons analogously to Fig. 2. *a–l*, representative micrographs of a GFP-WT neuron (*a–d*; *green*), a GFP-lacking DKO neuron (*e–h*), and a GFP-lacking DKO neuron co-cultured with WT neurons (*i–l*) immunostained for the γ2 subunit (*b*, *f*, and *j*; *red*) and GAD (*c*, *g*, and *k*; *blue*) with corresponding merged images shown in *d*, *h*, and *l*. *Boxed* dendritic segments of each image are shown enlarged in the *right-most column* with *arrows* pointing to colocalized pre- and postsynaptic structures of axons that have grown along dendrites and seem to adhere to dendrites and with *arrowheads* pointing to axons (*blue*) that have grown across dendrites with minimal contact, seemingly ignoring the dendrites. *m–p*, summary quantifications of the density of immunoreactive puncta for γ2 (*m*) and GAD (*n*), their colocalization (*o*), and the average size of γ2 puncta per neuron (*p*). Note the reduced density of pre- and postsynaptic puncta selectively in DKO neurons co-cultured with WT neurons, whereas the size of γ2 puncta was unaltered. Bar graphs with *error bars* indicate means ± S.E. ***, $p < 0.001$, ANOVA, Tukey tests. *Scale bar*, 5 μm.

(500 μM; 20 s) were unaffected (DKO, 931 ± 210 pA; WT, 1022 ± 234 pA; $p > 0.05$, $n = 12$, *t* test) (Fig. 4*b*). However, consistent with the reduced density of punctate $GABA_AR$ and GAD immunostaining, the frequency and amplitude of mIPSCs recorded from DKO neurons were significantly reduced compared with WT neurons (frequency mean values: DKO, 0.15 ± 0.08 Hz; WT, 0.24 ± 0.09 Hz; amplitude mean values: DKO, 19.9 ± 1.9 pA; WT, 22.5 ± 2.2 pA; $n = 12$ for both comparisons, $p < 0.05$, Kolmogorov-Smirnov test) (Fig. 4, *d* and *e*). Moreover, the frequency but not the amplitude of mEPSCs was reduced in DKO *versus* WT neurons (frequency: DKO, 0.65 ± 0.18 Hz; WT, 1.3 ± 0.51 Hz; $p < 0.00$, $n = 12$, Kolmogorov-Smirnov test; amplitude: DKO, 18.3 ± 2.4 pA; WT, 17.7 ± 2.1 pA; *p*, n.s.; $n = 12$, Kolmogorov-Smirnov test) (Fig. 4, *g* and *h*). Frequency changes of mEPSCs that are accompanied by unaltered mEPSC amplitudes can generally be attributed to altered neurotransmitter release probabilities of presynaptic terminals, which in our co-cultures primarily were derived largely from WT neurons. Moreover, we recently showed that modest defects in GABAergic synapses of $GABA_AR$ $\gamma2^{+/-}$ neurons result in a significant homeostatic-like reduction in the density of glutamatergic synapses (24), indicating that the change in mEPSC frequency recorded from DKO neurons was indirect and not indicative of altered palmitoylation of proteins functioning at glutamatergic synapses.

GODZ Is Essential for Palmitoylation of the $GABA_AR$ γ2 Subunit and GAP-43 in Vivo—Given the normal immunostaining of the γ2 subunit in pure GODZ KO and DKO cultures, it was critically important to ascertain whether GODZ KO mice suffered from measurable defects in palmitoylation *in vivo*. Candidate protein substrates of GODZ/SERZ-β based on PAT assays of transfected cells, in addition to the γ2 subunit, include GAP-43 (11). GAP-43 was of additional interest because it was recently identified as a gephyrin-interacting protein that regulates the degradation of gephyrin and, indirectly through altered gephyrin clustering, modulates the cell surface expression of $GABA_AR$s in developing neurons. Co-transfection of HEK293T cells with GAP-43 and GODZ resulted in significantly increased GAP-43 palmitoylation compared with transfection of GAP-43 alone (GODZ plus GAP-43, 620.4 ± 105.7% of GAP-43 alone) (Fig. 5*a*). Moreover, GODZ failed to palmitoylate a mutant version of GAP-43, $GAP\text{-}43^{C3S,C4S}$, that had its

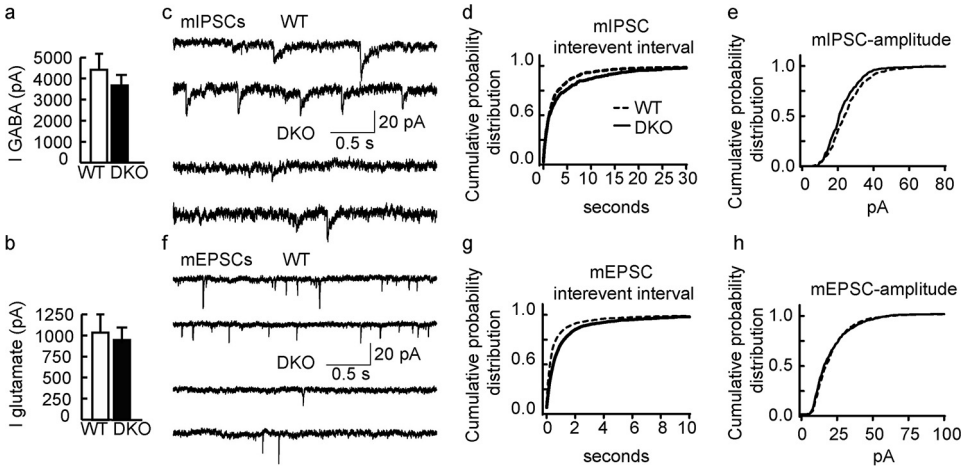

FIGURE 4. **Functional deficits of DKO neurons in inhibitory and excitatory neurotransmission.** *a* and *b*, DKO neurons grown in competition with WT neurons compared with WT neurons showed no significant change in whole-cell currents (*I*) evoked by GABA or glutamate ($p > 0.05$, $n = 12$ for both comparisons, *t* tests). *c*, representative traces of mIPSCs recorded from a WT (*top*) and a DKO neuron (*bottom*). *d* and *e*, cumulative probability plots of mIPSCs indicate longer interevent intervals ($p < 0.05$) (*d*) and a smaller amplitude ($p < 0.001$, $n = 12$, Kolmogorov-Smirnov test) (*e*) of mIPSCs in DKO compared with wild-type neurons. *f*, representative traces of mEPSCs recorded from a WT (*top*) and a DKO neuron (*bottom*). *g* and *h*, cumulative probability plots indicate that the interevent intervals (*g*) of mEPSCs were increased in DKO compared with WT neurons ($p < 0.001$), whereas the amplitude (*h*) was unaltered ($p > 0.05$, $n = 12$, Kolmogorov-Smirnov test). Bar graphs with *error bars* indicate means ± S.E.

putative palmitoylation sites changed to serine (GODZ plus GAP-43^{C3S,C4S}, 10.85 ± 2.85% of GAP-43 alone ($F(2,6) = 21.08$, $p < 0.01$, ANOVA; $p < 0.01$, $n = 3$ cultures for both comparisons, Tukey test) (Fig. 5, *a* and *b*). These experiments confirmed that GAP-43 is a substrate of GODZ *in vitro* and that GODZ-mediated palmitoylation is dependent on the known palmitoylation sites (Cys-3 and -4) of GAP-43 (25).

To assess whether the γ2 subunit and GAP-43 were dependent on GODZ for normal palmitoylation *in vivo*, we quantitated the steady state palmitoylation levels of these proteins by acyl-biotin exchange (ABE) assays of whole brain extracts of GODZ KO and WT mice. These assays involve blocking of the free cysteine residues of proteins with *N*-ethylmaleimide followed by hydrolyzing the thioester linkages between cysteine residues and palmitate with hydroxylamine and conjugating the newly freed cysteine residues to a cysteine-reactive biotin compound that then allows for pulldown of the previously palmitoylated proteins with streptavidin beads. Hydroxylamine-lacking reactions were routinely analyzed in parallel to qualitatively monitor unspecific labeling and pulldown of proteins independently of palmitate substitution. The amount of palmitoylated protein in the pulldown assay (hydroxylamine lanes) was quantitated by Western blotting using antibodies directed against the proteins of interest and normalizing to total amounts of the same proteins in aliquots of the same extracts on the same gel/Western blot. Based on such assays, steady state palmitoylation of both the γ2 subunit and GAP-43 was markedly decreased in GODZ KO *versus* WT brain (γ2: KO, 67.2 ± 4.7% of WT, $p < 0.001$, $n = 7–8$ mice; GAP-43: KO, 66.2 ± 12.2% of WT, $p < 0.05$, $n = 7$ mice, *t* tests) (Fig. 5*b*). Therefore, both the γ2 subunit and GAP-43 represent genuine substrates of GODZ *in vivo*. By contrast, palmitoylation of PSD-95 was unaffected (GODZ KO, 108.6 ± 10.1% of WT, $p = 0.589$, $n = 4$, *t* test) (Fig. 5*b*), although this protein can be readily palmitoylated by GODZ when enzyme and substrate are overexpressed in HEK293T cells (11). Similarly, palmitoylation of the AMPAR subunits GluA2/3 was unaltered in GODZ KO *versus* WT brain (KO, 104.4% ± 18.1% of WT, $n = 5$) even though these receptors can be palmitoylated by overexpression of recombinant GODZ (19). The total expression of γ2, GAP-43, and GluA2/3 (normalized to β-tubulin) was unaltered in KO mice (KO: γ2, 105.4 ± 15.4% of WT; GAP-43, 159.4 ± 32.9% of WT; GluA2/3, 82.4 ± 3.2% of WT; $n = 5$; *p*, n.s. for all three comparisons; *t* tests) (Fig. 5, *e* and *f*), indicating that differences apparent in ABE assays did not involve alterations in protein expression. Notably, there was a non-significant trend for increased expression of GAP-43 in KO *versus* WT brain ($p = 0.16$) that is consistent with reduced GABAergic inhibitory tone and evidence that GAP-43 expression is subject to neural activity-mediated up-regulation. Interestingly, neither palmitoylation of γ2 nor of GAP-43 or GluA2/3 was measurably reduced in brain extracts of SERZ-β KO mice (KO: γ2, 109.2 ± 20.4% of WT; GAP-43, 110.6 ± 11.2% of WT, GluA2/3, 96.7 ± 17.6% of WT; *p*, n.s; $n = 5$ for all three comparisons; *t* tests) (Fig. 5, *g* and *h*). Therefore, the *in vivo* substrates of GODZ and SERZ-β represent only a subset of the large number of proteins that can be palmitoylated by overexpression of the enzymes and substrates in heterologous cells.

GODZ and SERZ-β Are Dispensable for Cell Surface Accumulation of $GABA_ARs$—To independently assess whether GODZ and SERZ-β are required for accumulation of $GABA_A$Rs or AMPARs at the neuronal cell surface, we measured the expression of these proteins by cell surface biotinylation, starting with analyses of hippocampal brain slices. The cell surface values determined for the γ2 and GluA2/3 subunits in hippocampal brain slices of WT and GODZ KO were normalized to the amounts of β-tubulin determined in aliquots of total extracts from the same biotinylated brain samples set aside before affinity purification. We found no significant changes in the cell surface expression of γ2 and GluA2/3 subunits in GODZ KO mice (γ2, 104.8 ± 24.33% of WT, $p = 0.89$; GluA2/3,

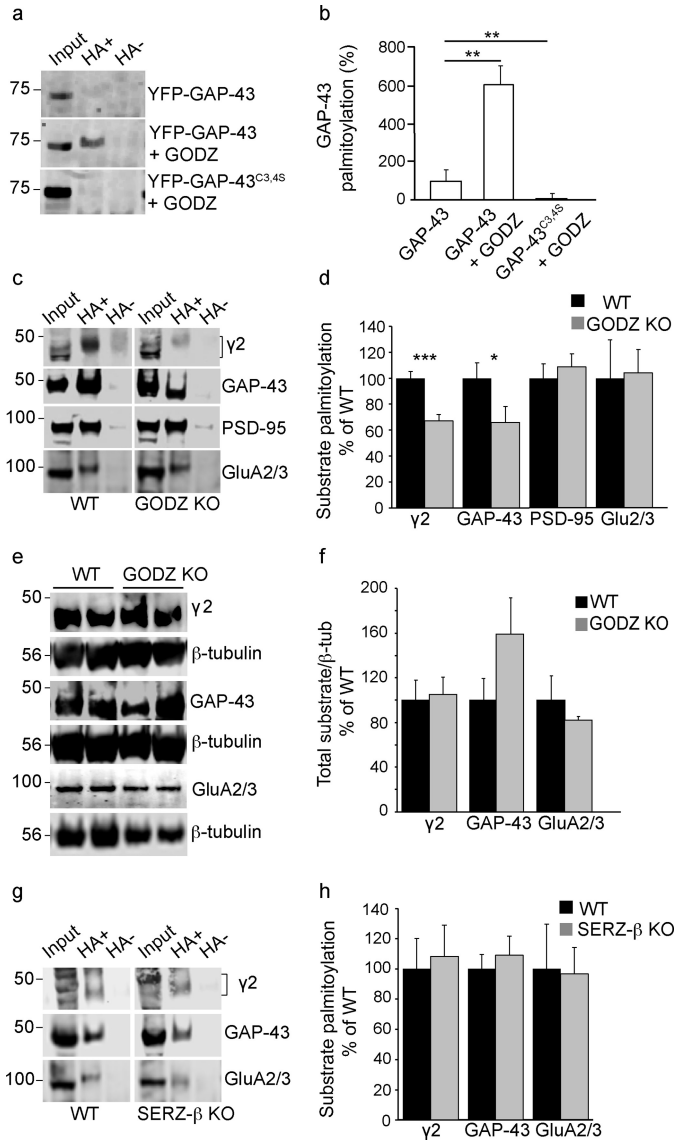

FIGURE 5. **GODZ KO mice exhibit reduced palmitoylation of GAP-43 and γ2-GABA$_A$Rs.** *a*, representative ABE assays of HEK293T cells transfected with either GFP-GAP-43 alone, GFP-GAP-43 with HA-GODZ, or GFP-GAP-43^{C3S,C4S} with HA-GODZ. *Input lanes* represent aliquots of assays removed before pull-down of biotinylated samples and used for normalization. Hydroxylamine-containing (*HA+*) lanes represent palmitoylated substrate, and hydroxylamine-lacking (*HA−*) lanes represent negative controls (see "Experimental Procedures"). *b*, summary quantification of data in *a* showing GODZ-induced palmitoylation in a GAP-43 Cys-3/4-dependent manner. *c* and *d*, representative ABE assays of brain extracts from GODZ KO and WT mice analyzed on the same gel (*c*) and summary quantification of substrate palmitoylation normalized to input and WT (*d*). Note the marked reductions in steady state palmitoylation of the γ2 subunit and GAP-43 and unaltered palmitoylation of PSD-95 and GluA2/3 subunits in brain of GODZ KO *versus* WT mice. *e* and *f*, representative Western blots comparing total brain extracts of two GODZ KO and two WT mice probed for the γ2 subunit, GAP-43, or GluA2/3 subunits (*e*). The three proteins were analyzed in separate aliquots of the same extracts. Parallel blots of the same extracts were probed for β-tubulin (*β-tub*) and used to normalize γ2, GAP-43, and GluA2/3 protein amounts for summary quantification (*f*). Note that the expression of γ2, GAP-43, and GluA2/3 was unchanged except for a weak trend for increased expression of GAP-43 in KO *versus* WT brain. *g* and *h*, ABE assays of WT and SERZ-β KO brain extracts analyzed on the same gel and probed for γ2, GAP-43, or GluA2/3 (*g*). Summary statistics (*h*) indicate that palmitoylation of all three proteins was unchanged in SERZ-β KO *versus* WT brain. Bar graphs with *error bars* indicate means ± S.E. *, $p < 0.05$; **, $p < 0.01$; ***, $p < 0.001$, *t* tests.

138.6 ± 31.0% of WT, $p = 0.29$; $n = 5$ mice per genotype for both comparisons; *t* tests) (Fig. 6, *a–d*).

Analogous cell surface biotinylation assays of hippocampal slices isolated from SERZ-β KO mice revealed that the cell surface expression of γ2 and GluA2/3 was unaltered also in SERZ-β KO mice (γ2, 103.4 ± 23.9% of WT, $p = 0.91$; GluA2/3, 57.9 ± 13.8% of WT, $p = 0.10$; $n = 5$ mice per genotype for both comparisons; *t* tests) (Fig. 6, *e–g*) except for a weak trend for down-regulation of GluA2/3 that was not confirmed in DKO neurons (see below).

To further assess the purity of cell surface-biotinylated protein fractions and to validate the negative results of the above experiments, we retroactively estimated an enrichment factor for GluA2/3 in cell surface-biotinylated *versus* total protein fractions using either β-tubulin or β-actin as a cytoplasmic reference protein (Fig. 6, *a* and *d*). Although β-tubulin was only partially reduced in cell surface fractions *versus* total extracts, β-actin was highly depleted and barely detectable in some cell surface fractions (Fig. 6, *a* and *d*). Thus, β-tubulin but not β-actin remains partially associated with cell surface-biotinylated, affinity-purified membrane fractions. To estimate an enrichment factor for cell surface proteins in cell surface-biotinylated *versus* total protein fractions, we first normalized the GluA2/3 expression level for both the cell surface and total fractions to the respective β-actin level. The average enrichment factor for cell surface-biotinylated protein fractions, defined as normalized surface GluA/total GluA, was 192 ± 82-fold ($n = 12$ brains). Analogous determination of a cell surface enrichment factor using normalization to β-tubulin instead of β-actin revealed an enrichment factor of 55 ± 26 ($n = 12$), confirming that β-tubulin remained partially associated with purified cell surface fractions.

SERZ-β Does Not Contribute to GABA$_A$R Trafficking and Function Even in the Absence of GODZ—To test for possible functional redundancy of GODZ and SERZ-β, we further examined primary cultured neurons prepared from DKO embryos. The cell surface expression levels of γ2 and GluA2/3 subunits were not measurably altered in DKO *versus* WT cultures (γ2, 109 ± 11.7% of WT; *p*, n.s.; $n = 5$; GluA2/3, 107.3 ± 9.0% of WT; *p*, n.s.; $n = 4$) (Fig. 6, *h–j*). The average cell surface enrichment factor in this experiment using normalization to β-tubulin was 7.8 ± 2.5-fold ($n = 8$ cultures). Unaltered cell surface expression of γ2 and GluA2/3 subunits in DKO is consistent with normal densities and sizes of postsynaptic γ2 puncta in pure DKO cultures (Fig. 3, *m* and *p*) and unaltered GABA- and glutamate-evoked whole-cell currents in DKO neurons of mixed genotype cultures (Fig. 4, *a* and *b*). Taken together, the results indicate that neither GODZ nor SERZ-β is essential for normal cell surface expression of GABA$_A$Rs nor do these PATs measurably regulate exocytosis of AMPARs or show any appreciable redundancy with respect to palmitoylation of these putative substrates. Although GODZ is essential for normal palmitoylation of the γ2 subunit and for accumulation of GABA$_A$Rs at synapses and GABA$_A$R-dependent presynaptic innervation, the detailed mechanism by which palmitoylation controls the trafficking or accumulation of these receptors at synapses remains ill-defined (see "Discussion").

GODZ and SERZ-β Are Differentially Restricted to cis- and trans-Golgi—The collective evidence so far has pointed to a selective role for GODZ in palmitoylation of the γ2 subunit and

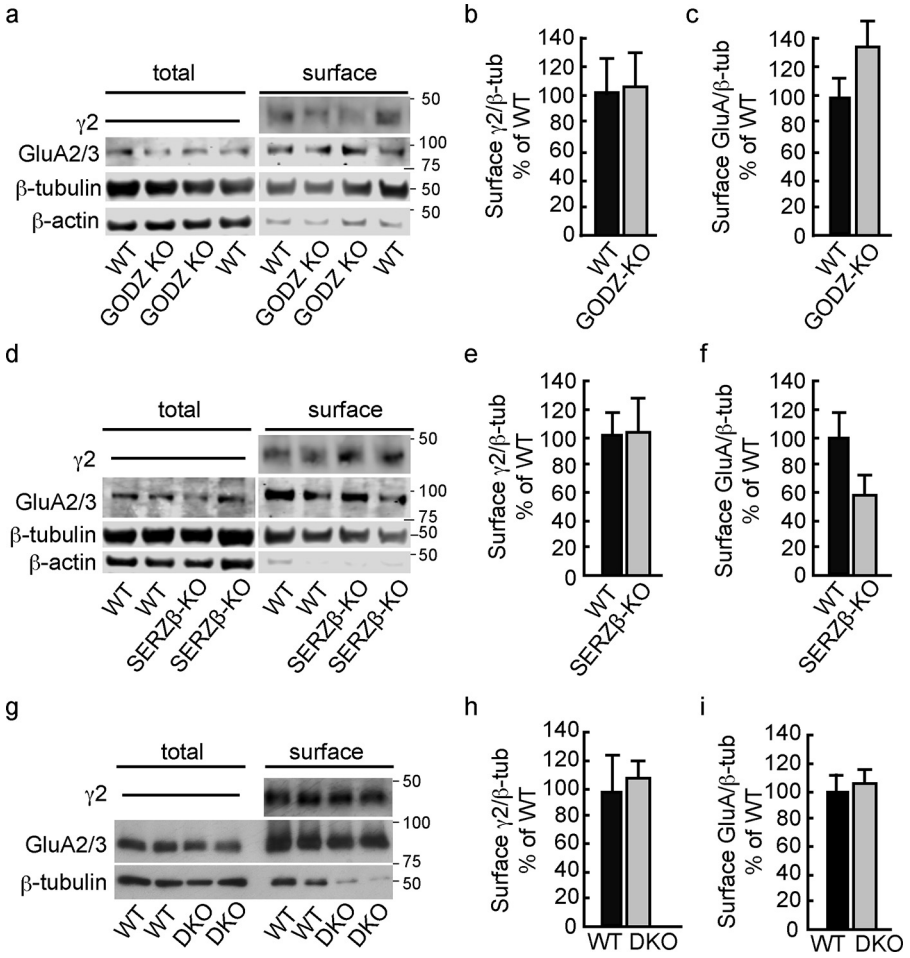

FIGURE 6. **Unaltered cell surface expression of $GABA_A$Rs and AMPARs in brain slices of KO mice and DKO neuron cultures.** *a–f*, cell surface-biotinylated protein fractions of hippocampal brain slices of GODZ KO (*a–c*) and SERZ-β KO mice (*d–f*) were analyzed for expression of the γ2 and GluA2/3 subunits of $GABA_A$Rs and AMPARs, respectively, and compared with respective fractions of WT littermates. Cell surface values were normalized to the amount of β-tubulin present in aliquots of total extracts set aside before pulldown of biotinylated cell surface proteins. In addition, the ratio of GluA2/3 to β-actin expression was compared in total *versus* cell surface fractions to estimate a cell surface enrichment factor for GluA2/3 subunits (see text for further details). Note the depletion of cell surface fractions of β-actin and the drastically increased ratio of GluA2/3/β-actin in cell surface *versus* total extracts of both experiments (*a* and *d*). By contrast, significant amounts of β-tubulin remained associated with affinity-purified cell surface fractions. Summary statistics of cell surface fractions normalized to β-tubulin revealed no significant differences in cell surface expression of γ2 (*b* and *e*) and GluA2/3 subunits (*c* and *f*) in GODZ KO (*b* and *c*) and SERZ-β KO mice (*e* and *f*) (p, n.s. for all four comparisons; *t* tests). *g–i*, analyses of cell surface-biotinylated protein fractions of cortical cultures prepared from WT and DKO embryos and probed for γ2 and GluA2/3 subunits. Duplicate aliquots of cell surface fractions and total extracts from pairs of WT and DKO cultures prepared and processed in parallel were compared on the same gel. The cell surface expression levels of γ2 (*h*) and GluA2/3 subunits (*i*) (normalized to β-tubulin (β-*tub*)) were not measurably altered in DKO *versus* WT cultures (p, n.s; *t* tests). Bar graphs with *error bars* indicate means ± S.E.

GAP-43 *in vivo*. Furthermore, although GODZ and SERZ-β show indistinguishable substrate specificity *in vitro* and neuron-specific expression in brain *in vivo* (18), SERZ-β was dispensable for normal palmitoylation of the γ2 subunit and GAP-43 *in vivo*. We wondered, therefore, whether functional differences between GODZ and SERZ-β might reflect subtle differences in the precise localization of these two enzymes in the Golgi complex. To address these questions, we first assessed the suborganellar localization of GODZ in the Golgi using transfection of HEK293T cells with either the cis/medial-Golgi marker N3 (also known as Golgi phosphoprotein of 130 kDa) fused to GFP (GFP-N3) or the trans-Golgi marker galactosyltransferase fused to YFP (YFP-GalT) (26, 27). Immunofluorescent images of cells stained for endogenous GODZ and the two Golgi markers were captured by super-resolution structure-illuminated microscopy (SIM) followed by intensity correlation analysis of their colocalization in the Golgi area (Fig. 7). Although GODZ appeared perfectly colocalized with the cis-Golgi marker GFP-N3, GODZ immunoreactivity was largely excluded from areas labeled by the trans-Golgi marker YFP-GalT (Fig. 7, *a* and *b*). The mean intensity correlation quotient (ICQ) for colocalization of GFP-N3 with GODZ (0.22 ± 0.017) was significantly greater than that for GalT-YFP and GODZ (0.078 ± 0.019, $p < 0.001$, $n = 7–9$, *t* test) (Fig. 7*g*), indicating that GODZ was 2.8-fold more restricted to the cis- than the trans-Golgi complex. To address whether Golgi localization was affected by overexpression of GODZ (and to replicate experimental conditions used for analyses of SERZ-β below), we repeated the above experiment using transfection of epitope-tagged GODZ (Fig. 7, *c* and *d*). HA-GODZ remained significantly more colocalized with GFP-N3 (ICQ = 0.302 ± 0.021) than with GalT-YFP (ICQ = 0.157 ± 0.017, $p < 0.001$, $n = 11–17$, *t* test) (Fig. 7*h*). However, the degree of colocalization of transfected HA-GODZ with the cis-Golgi marker

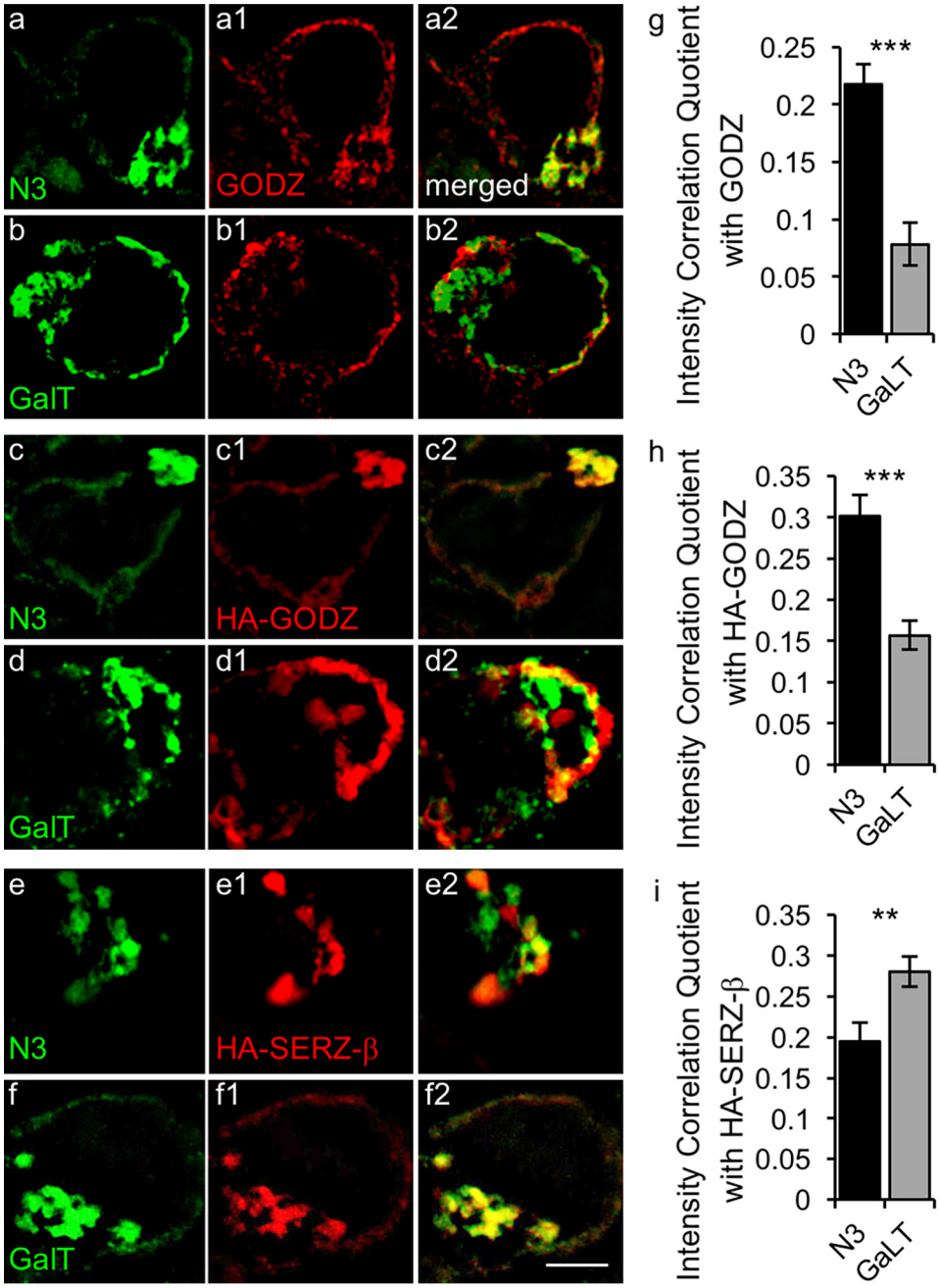

FIGURE 7. **Differential enrichment of GODZ and SERZ-β in cis *versus* trans compartment of the Golgi complex.** *a–f*, representative SIM images of HEK293T cells transfected with GFP-N3 (*a*, *c*, and *e*) or GalT-YFP (*b*, *d*, and *f*) together with HA-GODZ (*c* and *d*) or HA-SERZ-β (*e* and *f*). Cells were immunostained for GFP- or YFP-labeled Golgi markers (*a–f*; *green*) and either endogenous GODZ (*a1* and *b1*; *red*) or transfected HA-GODZ (*c1* and *d1*; *red*) or transfected HA-SERZ-β (*e1* and *f1*; *red*). Colocalization of the Golgi markers with GODZ or SERZ-β is evident in the merged images depicted in the *right-most column* (*a2–f2*; *yellow*). *g–i*, summary quantification of colocalization by intensity correlation analyses of immunofluorescence in the Golgi area for the indicated Golgi markers with endogenous GODZ (*g*), transfected HA-GODZ (*h*), and transfected HA-SERZ-β (*i*). Note that both endogenous GODZ and transfected HA-GODZ were strongly colocalized with the cis-Golgi marker GFP-N3 but not with the trans-Golgi marker GalT-YFP. By contrast, HA-SERZ-β showed greater colocalization with GalT-YFP than with GFP-N3. Bar graphs with *error bars* indicate means ± S.E. **, $p < 0.01$; ***, $p < 0.001$, *t* tests. *Scale bar*, 2.5 μm.

GFP-N3 was significantly reduced compared with corresponding colocalization of endogenous GODZ ($p < 0.05$, $n = 9–11$, ANOVA, Tukey test), suggesting ectopic localization of overexpressed GODZ in non-physiological cellar compartments. Importantly, corresponding analysis of HA-SERZ-β showed preferential localization of SERZ-β to the trans- rather than the cis-Golgi (ICQ(GalT-YFP/HA-SERZ-β) = 0.28 ± 0.018, ICQ(GFP-N3/HA-SERZ-β) = 0.19 ± 0.023, $p < 0.01$, $n = 15–16$, *t* test) (Fig. 7, *e*, *f*, and *i*). Thus, GODZ and SERZ-β are localized to different Golgi compartments, and the restricted localization of GODZ is compromised under assay conditions widely used in screenings for matching enzyme-protein substrate pairs.

Discussion

Here we have presented an initial characterization of GODZ and SERZ-β KO mice lacking expression of two of the most prominent members of the DHHC family of PATs that show

broad tissue distribution and that have garnered a reputation of largely indistinguishable and broad substrate specificity. Our studies confirm that GODZ is an important PAT for the γ2 subunit of $GABA_A$Rs and GAP-43, two proteins that contribute to inhibitory synapse function by entirely different mechanisms. The γ2 subunit is known to be required for postsynaptic clustering of $GABA_A$Rs and for GABAergic inhibitory synapse formation (28–30). This latter phenotype is specifically evident under competitive conditions, such as under artificial conditions where $\gamma2^{+/-}$ neurons are grown in competition with WT neurons (22) or following sparse *in utero* electroporation of embryonic cortex with a γ2 shRNA vector *in vivo* (30), and it may be physiologically relevant in the context of adult-born hippocampal neurons that must compete for innervation by axons of mature neurons (22). However, similar defects were not observed upon global deletion of the γ2 subunit in homogeneous γ2 KO cultures (28). Thus, reduced clustering of $GABA_A$Rs and defects in GABAergic innervation of GODZ KO neurons that were selectively observed in neurons grown in competition with WT neurons replicate the phenotype of γ2-deficient neurons grown in competitive conditions. The defect in inhibitory synapses observed in GODZ KO neurons is entirely consistent with moderately reduced expression of γ2-containing $GABA_A$Rs.

A putative role for GODZ-mediated palmitoylation of GAP-43 in the formation of GABAergic synapses, however, is more abstruse. There is general agreement that palmitoylation of GAP-43 is essential for its translocation from the Golgi to the plasma membrane, whereas its association with the plasma membrane can persist even after the protein has been depalmitoylated (for a review, see Ref. 31). GAP-43 is known to traffic through the cis-Golgi (32), which is consistent with restricted localization of GODZ specifically to this Golgi compartment. However, GAP-43 is subject to dynamic palmitoylation and depalmitoylation also at the plasma membrane as has been shown for GAP-43 localized to axonal growth cones (33). Given the restricted localization of GODZ to the cis-Golgi, this dynamic change in GAP-43 palmitoylation at the plasma membrane is likely mediated by PAT family members other than GODZ. More importantly, GAP-43 has recently been shown to associate with cytoplasmic gephyrin in a mechanism that is regulated by the phosphorylation state of a PKC site of GAP-43 (23). PKC-mediated phosphorylation of GAP-43 regulates the degree of cytoplasmic gephyrin aggregation and its sequestration into aggresomes and degradation, which in turn is thought to regulate the residual pool of gephyrin available for gephyrin-dependent clustering and stabilization of $GABA_A$Rs at inhibitory synapses (23). Although a direct mechanistic link between GODZ-mediated palmitoylation of GAP-43 and PKC-mediated phosphorylation of GAP-43 remains elusive, it is conceivable that defects in trafficking of GAP-43 through the early secretory pathway of GODZ KO neurons affect GAP-43 phosphorylation and hence contribute to impaired gephyrin- and $GABA_A$R-dependent formation of GABAergic synapses. However, much more elaborate experimentation would be needed to dissociate γ2-dependent from GAP-43-dependent defects in inhibitory synapse formation.

At the outset of our studies, we predicted that the mutant phenotype of GODZ KO mice might become compromised by functional redundancy between GODZ and SERZ-β, which prompted us to generate KO mice also for SERZ-β. These two PATs are not only closely related in their structure, they also exhibit largely indistinguishable substrate specificity when analyzed by overexpression of enzymes and putative substrates in transfected heterologous cells (6, 18) along with similar broad mRNA tissue distribution in peripheral tissues and similar neuron-specific expression in brain (11, 18). The absence of overt behavioral and physical phenotypes in single KO mice together with the severely runted or lethal phenotype of DKO mice supported our prediction that GODZ and SERZ-β show overlapping substrate specificity. However, we were surprised to find that the synaptic defects of DKO neurons were not more severe than those of GODZ KO neurons and that palmitoylation of γ2 and GAP-43 was perfectly normal in SERZ-β KO mice. We also noted that other paralogs of GODZ might contribute to $GABA_A$R and GAP-43 palmitoylation *in vivo* even though these enzymes were ineffective in palmitoylating these proteins in transfected HEK293T cells (11, 18). In particular, we found that the mRNA coding for the somewhat more distantly related GODZ/SERZ-β paralog DHHC15, as quantitated by RT-PCR, was significantly up-regulated in brain tissue of GODZ KO and DKO mice compared with WT littermate controls (DHHC15 mRNA in percentage of WT: GODZ KO, 129.3 ± 10.9% of WT, $p < 0.05$; DKO, 207.1 ± 40.1% of WT, $p < 0.05$; $n = 4$, *t* tests). Thus, DHHC15 could account for residual palmitoylation of γ2 and GAP-43 observed in GODZ KO mice even if it does not contribute to palmitoylation of these substrates in WT mice. By contrast, mRNA levels for yet another GODZ/SERZ-β paralog, DHHC21, were unchanged in DKO *versus* WT brain (not shown).

GODZ has previously been implicated as a PAT of PSD-95 (11) and AMPA receptor subunits GluA1–4 (19). However, we found that steady state palmitoylation of PSD-95 was unaffected in GODZ KO mice, which is consistent with convincing evidence that PSD-95 palmitoylation is mainly mediated by DHHC2 (13), DHHC5 (34), and DHHC8 (35). In the case of AMPA receptors, overexpression of GODZ was previously reported to limit the receptor cell surface expression in cultured neurons (19). If this effect of overexpressed GODZ was due to increased AMPAR subunit palmitoylation one would predict that GODZ KO mice would show increased cell surface expression of AMPA receptors. However, we found no measurable change in GluA2/3 palmitoylation and cell surface expression in GODZ KO and SERZ-β KO mice. Moreover, we found no change in the cell surface expression of GluA2/3 subunits, glutamate-evoked whole-cell currents, or mEPSC amplitudes in DKO cultured neurons, indicating that GODZ and SERZ-β do not regulate constitutive trafficking of AMPARs to the plasma membrane. Instead, reduced AMPAR cell surface expression seen following overexpressed GODZ is likely due to artificial mass-driven interaction with and trapping by GODZ in the Golgi compartment as we described previously for the γ2 subunit and shorter polypeptide substrates coexpressed with GODZ or SERZ-β in transfected cells (18). When overexpressed in heterologous cells, GODZ, SERZ-β, and their puta-

tive substrates form stable complexes in the Golgi region, seemingly reflecting trapping in a very limited membrane compartment where these substrates do not normally accumulate. Such complexes appear useful to map protein-protein interaction domains, but they interfere with the normal trafficking of substrates in a non-physiological manner (18). It is also noteworthy that GODZ DKO neurons grown in competition with WT neurons showed a slight reduction in the frequency of mEPSCs in DKO neurons that is reminiscent of GABAergic deficit-induced homeostatic down-regulation of glutamatergic synapses observed in $\gamma 2^{+/-}$ cultures and mice (24). Collectively, our studies indicate that the substrate specificity of GODZ is much narrower than previously thought, and they call for caution when interpreting DHHC enzyme-substrate relationships based on overexpression of these proteins in cultured cells.

The finding of unaltered $GABA_AR$ and GAP-43 palmitoylation in SERZ-β KO mice was unexpected and raised the question of whether SERZ-β and GODZ differed in their precise subcellular localization. Analyses by immunoelectron microscopy had previously suggested an asymmetric distribution of GODZ across the Golgi stack, but whether GODZ was restricted to the cis- or trans-face of the complex had remained elusive (18). The super-resolution imaging used here unambiguously identified GODZ as a cis-Golgi PAT, whereas SERZ-β was enriched in the trans-Golgi compartment. Moreover, we showed that overexpression of GODZ compromised its restricted localization to the cis-Golgi. It stands to reason then that the different substrate specificity of GODZ and SERZ-β is at least in part due to their differential localization in the secretory pathway.

None of the neuronal substrates examined in this study could be identified as genuine *in vivo* substrate of SERZ-β. However, we recently identified SERZ-β as a principal PAT for the glucose transporter GluT4 in adipocytes and muscle cells.[4] SERZ-β KO mice were shown to suffer from hyperglycemia and glucose intolerance, consistent with prominent defects in insulin-induced palmitoylation of GluT4 and translocation of GluT4 to the plasma membrane. GODZ and SERZ-β KO mice will be instrumental in evaluating the role these enzymes play in a range of physiological processes both in the CNS and in peripheral tissues.

Experimental Procedures

Animals—KO mice were generated by homologous recombination of the genomic loci in BK4 embryonic stem (ES) cells (37) using targeting vectors that contained a loxP site between the second and third protein-coding exons and a PGK-neo cassette flanked by a loxP site inserted between the fourth and fifth protein-coding exons of the genes and coding GODZ and SERZ-β (Fig. 1, *a* and *b*). Exons 3 and 4 encode the DHHC-CRD of each gene, which is known to be essential for PAT activity of DHHC family PATs (38). Deletion of exons 3 and 4 in each case is predicted to result in a shift of the reading frame downstream of the deleted exons. Thus, deletion of exons 3 and 4 of each gene is predicted to result in truncated proteins lacking the DHHC-CRD domains that are essential for PAT activity as well as all other sequences downstream of exon 2, most likely resulting in unstable proteins. The targeting vector for GODZ was derived from the bacterial artificial chromosome (BAC) clone RPCI-23-338G21 (BACPAC Resources Center, Children's Hospital Oakland Research Institute, Oakland, CA) and contained a 2999-bp NcoI-NheI left arm fragment with a loxP site at a unique EcoRI site (1098 bp from the NcoI site) followed by a loxP site-flanked PGK-neo cassette (inserted in the same transcriptional orientation as the target locus) and a 2951-bp NheI-EcoRI right arm fragment. Properly targeted ES cell clones (BK4 cell line (37); cells obtained from the Pennsylvania State University transgenic core) were screened and verified by Southern blotting and PCR, expanded and injected into blastocysts, and transferred to foster mothers following standard procedures of the Pennsylvania State University transgenic core facility. High grade chimeric offspring mice were then crossed with B6.FVB-Tg(EIIa-cre) C5379Lmgd/J mice (stock number 003724, The Jackson Laboratory, Bar Harbor, ME) to delete the loxP site-flanked exons and PGK-neo cassette. Offspring mice with germ line transmission and proper Cre-mediated deletion of the PGK-neo cassette (fGODZ locus; Fig. 1*a*) or both the PGK-neo cassette and exons 4 and 5 (GODZ KO allele; Fig. 1*a*) were identified by PCR analyses of genomic DNA of tail biopsies; the Cre transgene was subsequently removed by outcrossing. The recombined loci were confirmed by Southern blotting analyses of genomic DNA using probes that mapped to regions of the GODZ locus upstream and downstream of the targeting vector. SERZ-β KO mice were produced analogously using BAC RP23-87F1 as a source for generating the SERZ-β targeting vector (BACPAC Resources Center, Children's Hospital Oakland Research Institute). The "left arm" of the targeting vector consisted of a 2941-bp BglII fragment that was modified by insertion of a loxP site at a unique BamHI site (1307 bp downstream of the 5′ BglII site). This fragment was ligated to a PGK-neo cassette flanked by loxP sites with the PGK-neo cassette in the same transcriptional orientation as the SERZ-β locus followed by the "right arm" of the targeting vector consisting of a 4299-bp BglII-EcoRI genomic fragment. Properly targeted embryonic stem cells were identified and verified by genomic Southern blotting. High grade chimeric mice derived from these cells were crossed with Cre transgenic mice to delete the PGK-neo cassette as described above for GODZ KO mice, and the final floxed SERZ-β locus was verified in mice using Southern blotting and partial sequencing of PCR-amplified genomic fragments.

Husbandry and Genotyping of Mice—All mice were maintained on a standard 12:12 h light-dark cycle with food and water available *ad libitum*. The mice were maintained as heterozygotes on a 129-C57BL/6 mixed genetic background using brother-sister matings. KO mice used for experimentation were produced by mating of heterozygous mice, thereby allowing for experimental comparison with WT and heterozygous controls as littermates. All animal experiments were approved by the Institutional Animal Care and Use Committee of the Pennsylvania State University or by the Institutional Animal Care and Use Committee of the Tufts Medical Center and

[4] K. Du, S. Murakami, Y. Sun, C. Kilpatrick, and B. Luscher, manuscript under review.

performed in accordance with relevant guidelines and regulations of the National Institutes of Health. Routine genotyping of GODZ KO mice by PCR was done using primers GZ1 (5′-GAGGC TTCAG AATAG TCTCT TAC-3′) and GZ4 (5′-GCTCC CCAAC TCTTA CTTGA ATG-3′) for the mutant locus and primers GZ3 (5′-TGCCA GCCCA GCCTC ATTTT ATT-3′) and GZ4 (5′-GCTCC CCAAC TCTTA CTTGA ATG-3′) for the GODZ wild-type locus. SERZ-β KO mice were genotyped using the primers SZ1 (5′-TGAGC CAGGA TGGAT TTCAG ACA-3′) and SZ6 (5′TGCCC TCGGA CGCAG GAGAT GAA-3′) for the mutant locus and SZ4 (5′-TCCCC TGATG TATGC GAATG TCC-3′) and SZ5 (5′-AACAG GTGCC TTTTG AATGT CAG-3′). B5/EGFP mice (stock number 003516, The Jackson Laboratory) were genotyped as described (39).

Quantitation of mRNA by RT-PCR—Total RNA was isolated from brain using the TRIzol® Plus RNA Purification System (Thermo Fisher Scientific, Waltham, MA) and used for cDNA synthesis using the SuperScript® III First-Strand Synthesis System and oligo(dT) primer (Thermo Fisher Scientific). cDNAs were amplified using the following primers: GP1 (5′-CTAGA ATTCG CCACC ATGCT TATCC CCACC CATC-3′), GP2 (5′-GCAAT GCAGG AAGTG GAATC-3′), GP3 (5′-TCGAT AAGCT TGCGA CCACA TACTG GTACG GGTC-3′), SP1 (5′-CTAGA ATTCG CCACC ATGCA GCCGT CGGGA C-3′), SP2 (5′-TGCCC TCGGA CGCAG GAGAT GAA-3′), and SP3 (5′-AGTCT CGAGC TCAGA CAGAG AACTC GG-3′).

Western Blotting of Whole Brain Lysates—Mouse brains processed for quantification of GODZ and SERZ-β were lysed in SDS lysis buffer (50 mM Tris, pH 7.6, 10 mM NaP_2O_7, 100 nM NaF, 6 M urea, 10 mM EDTA, 10% (v/v) glycerol, and 2% (w/v) SDS). For quantification of γ2, GAP-43, or GluA2/3, the brain tissue was lysed in a buffer containing 150 mM NaCl, 50 mM Tris-HCl, pH 7.4, 5 mM EDTA, 1.7% Triton X-100, and protease inhibitors (Complete protease inhibitor mixture, Roche Applied Science). The tissue was homogenized three times for 15 s with a Powergen 125 homogenizer (Thermo Fisher Scientific), treated with a tip sonicator (Branson; three repeats of 9 s), and cleared of insoluble material by centrifugation (14,000 $\times$ *g*, 10 min). Immunoblots of supernatants analyzed by standard SDS-polyacrylamide gel electrophoresis (PAGE) were probed with rabbit antisera directed against the C-terminal 31-amino acid peptide of human GODZ (number sc-377378, Santa Cruz Biotechnology Inc., Dallas, TX), amino acids 40–193 of human SERZ-β (number SAB1101901, Sigma-Aldrich), an N-terminal peptide of the γ2 subunit (1:1000; number 224003, Synaptic Systems, Göttingen, Germany), and GAP-43 (1:1000; number AB5220, Millipore, Billerica, MA) and mouse anti-β-tubulin (1:1000; number T8535, Sigma-Aldrich). Analyses of total extracts for the γ2 subunit required analyses of separate protein aliquots without heat denaturation prior to SDS-PAGE to prevent aggregation.

Cell Surface Biotinylation—Cell surface biotinylation of cultured neurons was done as described previously (40). Briefly, two to three 6-cm culture dishes per genotype of DIV14 cortical neurons were incubated with (EZ-Link™ sulfo-NHS-SS-biotin, Thermo Fisher Scientific). The unreacted biotin was quenched by washing once with cold 50 mM glycine followed three times with 0.1% bovine serum albumin (BSA; number 7030, Sigma) in phosphate-buffered saline (PBS). The cells were lysed in ice-cold lysis buffer (150 mM NaCl, 10 mM Tris-HCl, pH 7.5, 1 mM EDTA, pH 8.0, 1% Triton X-100, 1 mM phenylmethylsulfonyl fluoride (PMSF), and 1 μg/ml each leupeptin, pepstatin A, antipain, and aprotinin), the protein was extracted for 15 min on ice, and the extracts were cleared by centrifugation at 10,000 $\times$ *g* for 10 min at 4 °C. Protein concentrations were determined using the Bradford (36) assay. Two hundred micrograms of protein were adsorbed to NeutrAvidin™ beads (Thermo Fisher Scientific) for 2 h at 4 °C, the beads were washed with lysis buffer (three times), and the bound protein were eluted with SDS-containing loading buffer. Duplicate aliquots of cell surface fractions and total extracts from matched pairs of WT and DKO cultures were analyzed by Western blotting analyses in five sequential experiments.

Biotinylation of brain slices was done as described (24). Briefly, 8–9-week-old mice were euthanized by cervical dislocation. Freshly isolated brains were rinsed with prechilled oxygenated artificial cerebrospinal fluid (ACSF) containing 124 mM NaCl, 3 mM KCl, 2 mM $CaCl_2$, 25 mM $NaHCO_3$, 1.1 mM NaH_2PO_4, 2 mM $MgSO_4$, and 10 mM D-glucose equilibrated with 95% O_2 and 5% CO_2 on ice and quickly sliced into 1-mm-thick coronal sections using a mouse brain matrix (stainless steel brain matrix, Stoelting Co., Wood Dale, IL). The sections containing the hippocampus were incubated in 1 mg/ml sulfo-NHS-SS-biotin (Thermo Fisher Scientific) in prechilled oxygenated ACSF and continuously equilibrated with 95% O_2 and 5% CO_2 on ice for 30 min. The tissue slices were washed with 50 mM glycine and 0.1% BSA in ACSF, and the regions of interest were isolated under a dissection microscope, triturated in lysis buffer, purified over NeutrAvidin beads, and processed for Western blotting as described above for cultures. The following antibodies were used: rabbit anti-γ2 (1:500; number G9919, Sigma-Aldrich or number 224 003, Synaptic Systems), rabbit anti-GluA2/3 (1:300; number AB1506, Millipore), mouse anti-β-tubulin (1:1000), and rabbit anti-β-actin (1:500; Sigma-Aldrich). Immunoblots were developed using IRDye and VRDye secondary antibodies and an Odyssey CLx infrared imager (LI-COR Biosciences, Lincoln, NE) and quantitated using Image Studio software (version 3.1; LI-COR Biosciences). Amounts of cell surface-biotinylated proteins were normalized to β-tubulin in total extracts quantitated on parallel gels.

ABE Assay—Extracts from brain tissue of 4-month-old mice or from transfected HEK293T cells were analyzed by the acyl-biotin exchange assay with minor modifications (41). The cells and tissues were lysed in LB buffer containing 150 mM NaCl, 50 mM Tris-HCl, pH 7.4, 5 mM EDTA, and 10 mM *N*-ethylmaleimide supplemented with protease inhibitors (Complete protease inhibitor mixture). Triton X-100 (1.7%) was added, and the tissue was homogenized using a tip sonicator (three 10-s pulses at 2.5 setting) followed by incubation on ice for 1 min. Proteins were diluted in LB buffer with 50 mM *N*-ethylmaleimide and incubated at 4 °C overnight with gentle rocking. Proteins were precipitated with chloroform/methanol, resolubilized in 4SB (4% SDS, 5 mM EDTA, and 50 mM Tris-HCl, pH 7.4) repeatedly. After the third precipitation, the samples were subjected to

Bradford (36) protein assays and adjusted to 2 mg/ml for HEK293T or 5 mg/ml for brain tissue and 400-μl volume with 4SB. An aliquot (2%) of each sample was saved as an input reference for later quantitation. The remainder of samples were diluted 5-fold with a buffer containing 1 mM EZ-Link *N*-[6-(biotinamido)hexyl]-3′-(2′-pyridyldithio)propionamide-biotin (number 21341, Thermo Fisher Scientific), 0.2% Triton X-100, 1× proteinase inhibitors, 1 mM phenylmethylsulfonyl fluoride, and either 0.7 M hydroxylamine, pH 7.4 (hydroxylamine reactions), or 50 mM Tris, pH 7.4 (hydroxylamine-lacking controls), for 1 h at room temperature. The proteins were precipitated with acetone three times; resuspended in 2% SDS, 5 mM EDTA, and 50 mM Tris-HCl, pH 7.4; adsorbed to high capacity streptavidin-agarose (number 20359, Thermo Fisher Scientific); washed; eluted off the beads using 200 mM DTT in LB buffer; separated by SDS-PAGE; and quantitated by Western blotting using primary antibodies directed against proteins of interest, IRDye-labeled secondary antibodies, and an Odyssey CLx laser scanner. Primary antibodies used were mouse anti-PSD-95 (1:1000; number MABN68, Millipore), rabbit anti-γ2 subunit (1:1000; No. 224003), and rabbit anti-GAP-43 (1:1000). For quantitation of substrate palmitoylation, the band intensities of hydroxylamine samples were subtracted by the band intensity of the corresponding hydroxylamine-lacking samples and then normalized to the amount of input protein analyzed in parallel on the same gel. Quantitation involved brain tissue of four to 11 mice per genotype or three independent cultures per condition in the case of transfected HEK293T cells.

Transfections—HEK293T cells (HEK293T/17, ATTC CRL 11268) used for palmitoylation experiments were obtained from ATCC (Manassas, VA) and cultured in high glucose Dulbecco's modified Eagle's medium (DMEM) with 10% fetal bovine serum (FBS) and 1% penicillin/streptomycin and transfected with plasmids using polyethyleneimine at a DNA to PEI ratio of 1:4, 1 μg of enzyme, and 4 μg of substrate plasmid per 6-cm Petri dish. The plasmids pEF-Bos-HA-DHHC3 and pEF-Bos-HA-DHHC7 encoding mouse GODZ and SERZ-β, respectively (11), were gifts from M. and Y. Fukata (National Institute for Physiological Sciences, Okazaki, Japan); pEGFP-GAP-43 and corresponding palmitoylation-deficient mutant constructs (42) were a gift from J. L. Daniotti, Universidad Nacional de Córdoba, Argentina; and pGPP130-GFP and pGalT-YFP (43, 44) were obtained from A. D. Linstedt, Carnegie Mellon University, Pittsburgh, PA.

Neuron Cultures—Cortical cultures were prepared from E14 mouse embryos essentially as described previously (22, 45) with the following modifications. For immunofluorescent stainings, the neurons were seeded on poly-L-lysine-coated coverslips at a density of 3.6×10^4 cells/cm^2. For mixed genotype cultures, dissociated GFP-transgenic wild-type neurons were mixed 9:1 with neurons obtained from GODZ KO or DKO embryos at the time of plating. After 24 h in culture, the coverslips were turned upside down and transferred to dishes containing glial feeder cells as described (45). For electrophysiological analyses, the dissected neurons were seeded at 1.7×10^5 cells/cm^2 at a ratio of GFP-WT/DKO neurons of 7:3 onto poly-D-lysine-coated coverslips covered by a monolayer of glial cells. The neuron cultures were maintained in a 10% CO_2 incubator except for electrophysiological recordings for which cells were maintained in 5% CO_2. Glial feeder cells were prepared from cortices of newborn rat pups as described (46).

Immunofluorescent Staining of Cultured Cells—Immunostaining of cultured neurons was performed at DIV18 after fixation and permeabilization as described (45) using the following primary antibodies: mouse anti-MAP2 (1:1000; Ab11267, Abcam), rabbit anti-GODZ directed against the C-terminal amino acids 250–299 of mouse GODZ (1:500; Ab31837, Abcam), mouse anti-gephyrin mAb7a (1:2000; a gift from H. Betz, Max Plank Institute, Frankfurt, Germany), guinea pig anti-$GABA_AR$ γ2 subunit (1:1500; a gift from Dr. J. M. Fritschy; Ref. 47), and mAb anti-glutamic acid decarboxylase 65/67 (0.5 μg/ml; Developmental Studies Hybridoma Bank, University of Iowa, Iowa City, IA). Immunostainings of doubly stained cultures were developed using appropriate combinations of secondary antibodies including Alexa Fluor 488-conjugated donkey anti-mouse, Alexa Fluor 647-conjugated goat anti-rabbit (1:500; Molecular Probes), and Cy3-conjugated donkey anti-guinea pig (1:500; Jackson ImmunoResearch Laboratories). Fluorescent images of pyramidal cell-like neurons were captured and digitized with a Zeiss Axiophot 2 microscope equipped with a 40× 1.3 NA objective and an ORCA-100 video camera (Hamamatsu) linked to an OpenLab imaging system (PerkinElmer Life Sciences). Digitized gray scale images representing different chromophores were pseudocolored, adjusted for contrast, and merged using OpenLab 5 (PerkinElmer Life Sciences) and assembled into figure palettes using Adobe Photoshop. Quantitation of the density and size of punctate immunoreactivities representative of synaptic proteins and the degree of colocalization of pre- and postsynaptic puncta was done with the investigator blinded to genotype essentially as described (24, 45). One or two properly innervated proximal dendritic segments of 40 μm in length were chosen from eight to nine cells per condition and selected from three or four independent experiments. Immunoreactive puncta representing pre- or postsynaptic clusters of proteins were automatically selected using OpenLab by utilizing a fluorescence intensity threshold corresponding to twice the diffuse fluorescence intensity measured on the shaft of the same dendrite and a target size range of 0.2–2 μm in diameter. To determine the percentage of colocalization between pre- and postsynaptic immunofluorescent puncta, the fraction of puncta for one protein that were maximally one pixel apart from puncta representing the other protein was counted in dendritic segments of 40 μm in length in proximity to the soma. The size (pixel numbers) of puncta was automatically recorded using OpenLab and used to calculate punctum area (1 pixel = 0.167 μm wide, 0.0279 μm^2 in area). Data were analyzed for normal distribution using the D'Agostino-Pearson test. Group means were compared by one-way ANOVA and Tukey post hoc tests.

Immunostaining of Brain Sections—Mice were anesthetized by intraperitoneal injection of Avertin (30 μl/g) (2,2,2-tribromoethanol (T48402, Sigma-Aldrich) in 2-methyl-2-butanol (152463, Sigma-Aldrich)), transcardially perfused with ice-cold PBS followed by 4% paraformaldehyde in PBS, and postfixed in the same solution at 4 °C for 12 h. Serial coronal brain sections (50 μm) were cut using a sliding microtome and permeabilized

with 1% Triton X-100 for 1 h followed by blocking for 1 h in 5% normal goat serum. The sections were incubated in rabbit anti-GODZ (directed against amino acids 250–299 of mouse GODZ; 1:500; Ab31837) and mouse anti-gephyrin mAb7a (1:2000; number 147 011, Synaptic Systems) overnight at 4 °C and developed using Alexa Fluor 488-conjugated anti-rabbit and Cy3-conjugated anti-mouse secondary antibodies. Fluorescent images were captured using an Olympus Fluoview 1000 confocal microscope equipped with a 40× 0.13 NA UPlanFL objective. Images were contrast-enhanced and assembled into figures using Adobe Photoshop.

Structured Illumination Microscopy and Intensity Correlation Analyses of Golgi Localization of GODZ/SERZ-β—HEK293T cells grown on poly-lysine-coated glass coverslips were transfected and immunostained essentially as described above using the plasmid GFP-N3 (43) or GalT-YFP (44) alone or together with HA-GODZ or HA-SERZ-β (11) (1 μg per plasmid), fixed, and immunostained using rabbit anti-GODZ (1:500; Ab31837) or rabbit anti-HA (1:1000; H6908, Sigma-Aldrich) and mouse anti-GFP (1:1000; A11120, Molecular Probes). Images were captured using a Nikon N-SIM microscope with a CFI Apochromat total internal reflection fluorescence 100× oil objective (NA 1.49) with Nikon Elements software utilizing the Center for Biologic Imagining (Pittsburgh, PA). Colocalization of transfected proteins was analyzed using ImageJ (National Institutes of Health, Bethesda, MD). The images were background-subtracted using the Subtract Background from region of interest plug-in followed by quantitation of colocalization with the Intensity Correlation analysis plug-in (48).

Electrophysiology—Cortical neurons at DIV9–11 were used for electrophysiological analyses. Whole-cell recordings were performed using Multiclamp 700A (Molecular Devices Corp., Sunnyvale, CA). The recording chamber was continuously perfused with a bath solution containing 128 mM NaCl, 30 mM D-glucose, 25 mM HEPES, 5 mM KCl, 2 mM $CaCl_2$, and 1 mM $MgCl_2$, pH 7.3 (adjusted using NaOH). Patch pipettes were filled with 147 mM KCl, 5 mM disodium phosphocreatine, 2 mM EGTA, 10 mM HEPES, 2 mM MgATP, and 0.3 mM Na_2GTP, pH 7.3 (adjusted with KOH). Data were acquired using PCLAMP 8 software, sampled at 10 kHz, and filtered at 1–2 kHz. To assess whole-cell currents, pulses (20 s) of GABA (100 μM) or glutamate (500 μM) were applied through a glass pipette with the pipette tip close to the cell soma, and evoked currents were recorded with the membrane potential clamped at −70 mV. Current peak amplitudes were measured using Clampfit 9 software (Molecular Devices Corp.) to obtain $GABA_A$ or AMPA receptor-mediated whole-cell currents (pA). mIPSCs and mEPSCs were recorded in the presence of 0.5 μM tetrodotoxin and either 10 μM 6-cyano-7-nitoquinoxaline-2,3-dione or 20 μM bicuculline, respectively.

Statistical Analysis—Statistical comparisons of multiple means of biochemical and imaging data were performed using Prism software (GraphPad, La Jolla, CA). Multiple comparisons were done by one-way ANOVA followed by Tukey post hoc analysis. Normality of data distribution of imaging data was assessed by D'Agostino-Pearson test. Simple comparison of two group means was done by two-sample two-tailed *t* tests. Analyses of miniature current data were performed using MiniAnalysis software (Synaptosoft, Decatur, GA) using Kolmogorov-Smirnov test. *p* values <0.05 were deemed significant.

Author Contributions—S. M. generated the KO mice and performed experiments depicted in Figs. 1, *a–c*; 6, *g–i*; and 4. C. L. K. performed experiments described in Figs. 1, *e* and *f*; 5; and 7. S. M. and R. L. performed experiments in Figs. 2 and 3. S. M. and M. F. performed experiments in Fig. 6. K. D. performed experiments in Fig. 1*d*. X. W. and G. C. performed and analyzed experiments described in Fig. 4. B. L. conceived and coordinated the study and together with C. L. K. wrote the paper. All authors reviewed the results and approved the final version of the manuscript.

Acknowledgments—We thank the members of the Pennsylvania State University transgenic mouse facility for performing blastocyst injections; Simon Watkins (Center for Biologic Imaging, University of Pittsburgh) for access and technical support in using the SIM microscope; and Sue Lingenfelter, Anjuli Datta and Yao Guo for technical assistance. Finally, we are grateful to Adam Linstedt, Masaki and Yuko Fukata, and Jose-Luis Daniotti for plasmid DNAs and Jean-Marc Fritschy and Heinrich Betz for gifts of antibodies.

References

1. Resh, M. D. (2006) Trafficking and signaling by fatty-acylated and prenylated proteins. *Nat. Chem. Biol.* **2,** 584–590
2. Greaves, J., and Chamberlain, L. H. (2007) Palmitoylation-dependent protein sorting. *J. Cell Biol.* **176,** 249–254
3. Salaun, C., Greaves, J., and Chamberlain, L. H. (2010) The intracellular dynamic of protein palmitoylation. *J. Cell Biol.* **191,** 1229–1238
4. Blaskovic, S., Blanc, M., and van der Goot, F. G. (2013) What does S-palmitoylation do to membrane proteins? *FEBS J.* **280,** 2766–2774
5. Kang, R., Wan, J., Arstikaitis, P., Takahashi, H., Huang, K., Bailey, A. O., Thompson, J. X., Roth, A. F., Drisdel, R. C., Mastro, R., Green, W. N., Yates, J. R., 3rd, Davis, N. G., and El-Husseini, A. (2008) Neural palmitoyl-proteomics reveals dynamic synaptic palmitoylation. *Nature* **456,** 904–909
6. Fukata, Y., and Fukata, M. (2010) Protein palmitoylation in neuronal development and synaptic plasticity. *Nat. Rev. Neurosci.* **11,** 161–175
7. Greaves, J., and Chamberlain, L. H. (2011) DHHC palmitoyl transferases: substrate interactions and (patho)physiology. *Trends Biochem. Sci.* **36,** 245–253
8. Korycka, J., Łach, A., Heger, E., Bogusławska, D. M., Wolny, M., Toporkiewicz, M., Augoff, K., Korzeniewski, J., and Sikorski, A. F. (2012) Human DHHC proteins: a spotlight on the hidden player of palmitoylation. *Eur. J. Cell Biol.* **91,** 107–117
9. Jennings, B. C., and Linder, M. E. (2012) DHHC protein *S*-acyltransferases use similar ping-pong kinetic mechanisms but display different acyl-CoA specificities. *J. Biol. Chem.* **287,** 7236–7245
10. Gottlieb, C. D., Zhang, S., and Linder, M. E. (2015) The cysteine-rich domain of the DHHC3 palmitoyltransferase is palmitoylated and contains tightly bound zinc. *J. Biol. Chem.* **290,** 29259–29269
11. Fukata, M., Fukata, Y., Adesnik, H., Nicoll, R. A., and Bredt, D. S. (2004) Identification of PSD-95 palmitoylating enzymes. *Neuron* **44,** 987–996
12. Ho, G. P., Selvakumar, B., Mukai, J., Hester, L. D., Wang, Y., Gogos, J. A., and Snyder, S. H. (2011) S-Nitrosylation and S-palmitoylation reciprocally regulate synaptic targeting of PSD-95. *Neuron* **71,** 131–141
13. Fukata, Y., Dimitrov, A., Boncompain, G., Vielemeyer, O., Perez, F., and Fukata, M. (2013) Local palmitoylation cycles define activity-regulated postsynaptic subdomains. *J. Cell Biol.* **202,** 145–161
14. Ohno, Y., Kihara, A., Sano, T., and Igarashi, Y. (2006) Intracellular localization and tissue-specific distribution of human and yeast DHHC cysteine-rich domain-containing proteins. *Biochim. Biophys. Acta* **1761,** 474–483

15. Uemura, T., Mori, H., and Mishina, M. (2002) Isolation and characterization of Golgi apparatus-specific GODZ with the DHHC zinc finger domain. *Biochem. Biophys. Res. Commun.* **296,** 492–496
16. Chaudhary, J., and Skinner, M. K. (2002) Identification of a novel gene product, Sertoli cell gene with a zinc finger domain, that is important for FSH activation of testicular Sertoli cells. *Endocrinology* **143,** 426–435
17. Keller, C. A., Yuan, X., Panzanelli, P., Martin, M. L., Alldred, M., Sassoè-Pognetto, M., and Lüscher, B. (2004) The γ2 subunit of $GABA_A$ receptors is a substrate for palmitoylation by GODZ. *J. Neurosci.* **24,** 5881–5891
18. Fang, C., Deng, L., Keller, C. A., Fukata, M., Fukata, Y., Chen, G., and Lüscher, B. (2006) GODZ-mediated palmitoylation of $GABA_A$ receptors is required for normal assembly and function of GABAergic inhibitory synapses. *J. Neurosci.* **26,** 12758–12768
19. Hayashi, T., Rumbaugh, G., and Huganir, R. L. (2005) Differential regulation of AMPA receptor subunit trafficking by palmitoylation of two distinct sites. *Neuron* **47,** 709–723
20. Hayashi, T., Thomas, G. M., and Huganir, R. L. (2009) Dual palmitoylation of NR2 subunits regulates NMDA receptor trafficking. *Neuron* **64,** 213–226
21. Oku, S., Takahashi, N., Fukata, Y., and Fukata, M. (2013) *In silico* screening for palmitoyl substrates reveals a role for DHHC1/3/10 (zDHHC1/3/11)-mediated neurochondrin palmitoylation in its targeting to Rab5-positive endosomes. *J. Biol. Chem.* **288,** 19816–19829
22. Ren, Z., Sahir, N., Murakami, S., Luellen, B. A., Earnheart, J. C., Lal, R., Kim, J. Y., Song, H., and Luscher, B. (2015) Defects in dendrite and spine maturation and synaptogenesis associated with an anxious-depressive-like phenotype of GABAA receptor-deficient mice. *Neuropharmacology* **88,** 171–179
23. Wang, C. Y., Lin, H. C., Song, Y. P., Hsu, Y. T., Lin, S. Y., Hsu, P. C., Lin, C. H., Hung, C. C., Hsu, M. C., Kuo, Y. M., Lee, Y. J., Hsu, C. Y., and Lee, Y. H. (2015) Protein kinase C-dependent growth-associated protein 43 phosphorylation regulates gephyrin aggregation at developing GABAergic synapses. *Mol. Cell. Biol.* **35,** 1712–1726
24. Ren, Z., Pribiag, H., Jefferson, S. J., Shorey, M., Fuchs, T., Stellwagen, D., and Luscher, B. (2016) Bidirectional homeostatic regulation of a depression-related brain state by γ-aminobutyric acidergic deficits and ketamine treatment. *Biol. Psychiatry* **80,** 457–468
25. Liu, Y., Fisher, D. A., and Storm, D. R. (1993) Analysis of the palmitoylation and membrane targeting domain of neuromodulin (GAP-43) by site-specific mutagenesis. *Biochemistry* **32,** 10714–10719
26. Strous, G. J. (1986) Golgi and secreted galactosyltransferase. *CRC Crit. Rev. Biochem.* **21,** 119–151
27. Linstedt, A. D., Mehta, A., Suhan, J., Reggio, H., and Hauri, H. P. (1997) Sequence and overexpression of GPP130/GIMPc: evidence for saturable pH-sensitive targeting of a type II early Golgi membrane protein. *Mol. Biol. Cell* **8,** 1073–1087
28. Essrich, C., Lorez, M., Benson, J. A., Fritschy, J.-M., and Lüscher, B. (1998) Postsynaptic clustering of major $GABA_A$ receptor subtypes requires the γ2 subunit and gephyrin. *Nat. Neurosci.* **1,** 563–571
29. Schweizer, C., Balsiger, S., Bluethmann, H., Mansuy, I. M., Fritschy, J. M., Mohler, H., and Lüscher, B. (2003) The γ2 subunit of $GABA_A$ receptors is required for maintenance of receptors at mature synapses. *Mol. Cell. Neurosci.* **24,** 442–450
30. Li, R. W., Yu, W., Christie, S., Miralles, C. P., Bai, J., Loturco, J. J., and De Blas, A. L. (2005) Disruption of postsynaptic GABA receptor clusters leads to decreased GABAergic innervation of pyramidal neurons. *J. Neurochem.* **95,** 756–770
31. Denny, J. B. (2006) Molecular mechanisms, biological actions, and neuropharmacology of the growth-associated protein GAP-43. *Curr. Neuropharmacol.* **4,** 293–304
32. Appenzeller-Herzog, C., and Hauri, H. P. (2006) The ER-Golgi intermediate compartment (ERGIC): in search of its identity and function. *J. Cell Sci.* **119,** 2173–2183
33. Skene, J. H., and Virág, I. (1989) Posttranslational membrane attachment and dynamic fatty acylation of a neuronal growth cone protein, GAP-43. *J. Cell Biol.* **108,** 613–624
34. Brigidi, G. S., Santyr, B., Shimell, J., Jovellar, B., and Bamji, S. X. (2015) Activity-regulated trafficking of the palmitoyl-acyl transferase DHHC5. *Nat. Commun.* **6,** 8200
35. Mukai, J., Dhilla, A., Drew, L. J., Stark, K. L., Cao, L., MacDermott, A. B., Karayiorgou, M., and Gogos, J. A. (2008) Palmitoylation-dependent neurodevelopmental deficits in a mouse model of 22q11 microdeletion. *Nat. Neurosci.* **11,** 1302–1310
36. Bradford, M. M. (1976) A rapid and sensitive method for the quantitation of microgram quantities of protein utilizing the principle of protein-dye binding. *Anal. Chem.* **72,** 248–254
37. Ito, M., Oliverio, M. I., Mannon, P. J., Best, C. F., Maeda, N., Smithies, O., and Coffman, T. M. (1995) Regulation of blood pressure by the type 1A angiotensin II receptor gene. *Proc. Natl. Acad. Sci. U.S.A.* **92,** 3521–3525
38. Lobo, S., Greentree, W. K., Linder, M. E., and Deschenes, R. J. (2002) Identification of a Ras palmitoyltransferase in *Saccharomyces cerevisiae*. *J. Biol. Chem.* **277,** 41268–41273
39. Hadjantonakis, A. K., Gertsenstein, M., Ikawa, M., Okabe, M., and Nagy, A. (1998) Generating green fluorescent mice by germline transmission of green fluorescent ES cells. *Mech. Dev.* **76,** 79–90
40. Yuan, X., Yao, J., Norris, D., Tran, D. D., Bram, R. J., Chen, G., and Luscher, B. (2008) Calcium-modulating cyclophilin ligand regulates membrane trafficking of postsynaptic $GABA_A$ receptors. *Mol. Cell. Neurosci.* **38,** 277–289
41. Wan, J., Roth, A. F., Bailey, A. O., and Davis, N. G. (2007) Palmitoylated proteins: purification and identification. *Nat. Protoc.* **2,** 1573–1584
42. Trenchi, A., Gomez, G. A., and Daniotti, J. L. (2009) Dual acylation is required for trafficking of growth-associated protein-43 (GAP-43) to endosomal recycling compartment via an Arf6-associated endocytic vesicular pathway. *Biochem. J.* **421,** 357–369
43. Mukhopadhyay, S., Bachert, C., Smith, D. R., and Linstedt, A. D. (2010) Manganese-induced trafficking and turnover of the cis-Golgi glycoprotein GPP130. *Mol. Biol. Cell* **21,** 1282–1292
44. Jarvela, T., and Linstedt, A. D. (2012) Irradiation-induced protein inactivation reveals Golgi enzyme cycling to cell periphery. *J. Cell Sci.* **125,** 973–980
45. Alldred, M. J., Mulder-Rosi, J., Lingenfelter, S. E., Chen, G., and Lüscher, B. (2005) Distinct gamma2 subunit domains mediate clustering and synaptic function of postsynaptic GABAA receptors and gephyrin. *J. Neurosci.* **25,** 594–603
46. Banker, G., and Goslin, K. (eds) (1998) *Culturing Nerve Cells*, 2nd Ed., The MIT Press, Cambridge, MA
47. Fritschy, J. M., and Mohler, H. (1995) GABAA-receptor heterogeneity in the adult rat brain: differential regional and cellular distribution of seven major subunits. *J. Comp. Neurol.* **359,** 154–194
48. Li, Q., Lau, A., Morris, T. J., Guo, L., Fordyce, C. B., and Stanley, E. F. (2004) A syntaxin 1, $G\alpha_o$, and N-type calcium channel complex at a presynaptic nerve terminal: analysis by quantitative immunocolocalization. *J. Neurosci.* **24,** 4070–4081